Secrecy Performance Analysis of Half/Full Duplex AF/DF Relaying in NOMA Systems Over κ - μ Fading Channels

Nesrine Zaghdoud (nesrine.zaghdoud@supcom.tn)
SupCom: Universite de Carthage Ecole Superieure des Communications de Tunis
https://orcid.org/0000-0002-6918-320X
Adel Ben Mnaouer
Canadian University of Dubai
Hatem Boujemaa
SupCom: Universite de Carthage Ecole Superieure des Communications de Tunis
Farid Touati
Qatar University

Research Article

Keywords: Physical layer security, NOMA, Full-duplex, Half-duplex, Amplify-and-Forward, Decode-and-Forward, Fading, κ - μ distribution

Posted Date: March 9th, 2021

DOI: https://doi.org/10.21203/rs.3.rs-218631/v1

Noname manuscript No.
(will be inserted by the editor)

Secrecy Performance Analysis of Half/Full Duplex AF/DF relaying in NOMA Systems over $\kappa - \mu$ fading Channels

Nesrine Zaghdoud[1,2] · **Adel Ben Mnaouer**[2] · **Hatem Boujemaa**[1] · **Farid Touati**[3]

Received: date / Accepted: date

Abstract Although the progress in understanding 5G and beyond techniques such as Non-Orthogonal Multiple Access (NOMA) and full-duplex techniques has been overwhelming, still analyzing the security aspects of such systems under different scenarios and settings is an important concern that needs further exploration. In particular, when considering fading in wiretap channels and scenarios, achieving secrecy has posed many challenges. In this context, we propose to study the physical layer security (PLS) of cooperative NOMA (C-NOMA) system using the general fading distribution $\kappa - \mu$. This distribution facilitates mainly the effect of light-of-sight as well as multipath fading. It also includes multiple distributions as special cases like: Rayleigh, Rice, Nakagami-m which help to understand the comportment of C-NOMA systems under different fading parameters. The use of Half-Duplex and Full-Duplex communication is also investigated for both Amplify-and-forward (AF) and Decode-and-Forward (DF) relaying protocols. To characterize the secrecy performance of the proposed C-NOMA systems, closed form expressions of the Secrecy Outage Probability (SOP) and the Strictly Positive Secrcey Capacity (SPSC) metrics for the strong and weak users are given for high signal-to-noise ratio (SNR) due to the intractable nature of the exact expressions. Based on the analytical analysis, numerical and simulation results are given under different network parameters.

Keywords Physical layer security · NOMA · Full-duplex · Half-duplex · Amplify-and-Forward · Decode-and-Forward · Fading · $\kappa - \mu$ distribution

✉ Nesrine Zaghdoud
nesrine.zaghdoud@supcom.tn

Adel Ben Mnaouer
adel@cud.ac.ae

Hatem Boujemaa
boujemaa.hatem@supcom.tn

Farid Touati
touatif@qu.edu.qa

[1] University of Carthage, SUPCOM, LR11TIC01 COSIM Research Lab, 2083, Ariana, Tunisia

[2] Faculty of Engineering and Architecture Canadian University Dubai, UAE

[3] Department of Electrical Engineering, Qatar University, Doha, Qatar

1 Introduction

For the previous mobile network generation (1G to 4G), Orthogonal Multiple Access (OMA) techniques were a practical choice to share the available channels for data transmission due to its simple protocol design and the relatively low-interference effect on users' communication. However, the number of users supported in OMA systems is restricted by the number of available orthogonal resources and with the exponential growth of mobile communications, OMA will be insufficient to support the challenging requirements of the next-generation of wireless communication [1].

Regarding the drawbacks of prior multiple access techniques, the innovative concept of NOMA promises a significant improvement in the system capacity, user fairness

and connectivity compared with OMA [2, 3]. NOMA techniques are divided in two categories based on code or power domain. Mainly, power domain is the widest used scheme. It allocates lower power to the strong NOMA users those having higher channel gain and more power to the weak users with poor channel condition in order to simultaneously serve multiple users. This leads to a significant fairness between NOMA users. To distinguish users' signal, NOMA takes advantage of the successive interference cancellation technique (SIC). Specifically, the strong channel user applies SIC to decode its own message by treating the message of other users as interference, while weak users signals are obtained by considering strong users signal as a noise [4, 5].

In addition, cooperative techniques coupled with NOMA, have revealed significant performance gains [6, 7]. Among the available cooperative schemes, dedicated relaying techniques have been proven to improve spatial and spectrum diversity, especially when no direct channel exists between communicating nodes or when a huge number of cell edge users have to be served . Different strategies such as Amplify and forward (AF) and decode and forward (DF) protocols are usually used especially for taking advantage from spatial diversity without requiring multiple antennas at the transmitter [8, 9]. In [10–13], downlink cooperative NOMA relying system based AF and DF strategies revealed better spectral efficiency and outage probability than conventional cooperative relaying system.

The advances in interference cancelation technique was not only the key behind the significant research progress on NOMA, but also for considering Full-duplex (FD) technology as one of the promising techniques for 5G and beyond systems proved to potentially double the spectral efficiency compared to the conventional Half-duplex communications. The integration of NOMA and FD technology was studied in [14–18] showing significant improvement in spectral efficiency compared to conventional wireless communications based on HD mode and OMA schemes.

The increased growth of wireless networks presents a significant challenge as it is intrinsically a broadcast and mobile based medium, which allows easy access to the transmitted data and makes it extremely harmful for ensuring confidentiality and privacy in such networks [19,20]. Generally, cryptographic techniques are presented as the conventional way to protect communication security by assuming that there exists a secret key shared between the transmitter and legitimate receivers. Thus, security is achieved based on the complexity of implementation of the secret keys and the available computational power and time of the attack. Although, in this era of 5G and beyond networks where massive number of devices with high computational capacity, maintaining security only using cryptographic techniques is hard to achieve [21, 22]. This leads to a new approach based on information theory introduced by Shanon and extended by the work of Wyner called physical layer security (PLS) [23, 24]. This approach exploits the physical characteristics of the wireless environment to ensure that no information is released to the eavesdropper where no limit on computational and time resources is considered.

Recent research considers PLS approach as a promising solution for enhancing security in 5G and beyond networks [25–27]. In [28], the secrecy outage probability (SOP) and the strictly positive secrecy capacity (SPSC) were evaluated for C-NOMA systems by considering both AF and DF protocols over Rayleigh fading channels. In [29], the strong user is considered as a DF relay and the SOP of both strong and weak NOMA users were derived, showing that optimal security can be achieved via an appropriate power control at the source and the strong user. Authors in [30] analyzed the secrecy outage performance of DF NOMA system over Nakagami-m fading channels, their results showed the SOP of NOMA system outperforms that of OMA system in the low and medium SNR region. In [31], the secrecy performance of a cooperative NOMA network with one relay operating in HD or FD used to decode and forward the weak user message was investigated in Rayleigh fading channels. Their results showed that the HD relay offers more secrecy than the FD relay. In [32], the use of artificial noise and FD strategies at the relay node to enhance the secrecy in NOMA cooperative networks was investigated. Results showed that the proposed system grants more secrecy than the use of artificial noise and HD strategies. In [33, 34], the secrecy outage of cooperative NOMA system assisted by a multi-antenna FD DF relay was investigated, the results showed that the secrecy can significantly be improved through the proposed multi-antenna FD relay and jamming scheme. Despite the significant aforementioned contributions on the secrecy performance of NOMA system, most of them studied secrecy over Rayleigh fading distribution, and few works investigated other fading models like Rice and Nakagami-m. Since, fading is one of the key concept of PLS [35], we propose to analyze secrecy over the generalized fading channel $\kappa - \mu$ [36, 37] which is suitable to model different fading scenario to gain more insight on its effect on the secrecy performance of NOMA system. The contribtions of the paper are:

- We analyze the effect of HD and FD relaying on the security of cooperative NOMA system for both AF/DF relaying protocols.
- We derive novel expressions of the secrecy outage probability and the strictly positive secrecy capacity of both strong and weak NOMA users for each of the studied scenarios over $\kappa - \mu$ fading channels.
- Finally, we confirm our analytical findings with Montecarlo simulations and numerical results to investigate the security of our system under different network parameters.

The rest of the paper is organized as follows. We describe the proposed system model in Section 2. The analytical analysis of the SOP is provided in Section 3. In Section 4, we detail analytical analysis of of the SPSC. We evaluate the performance and the correctness of the obtained analytical results in Section 5. Finally, in Section 6 we conclude the paper and provide directions for future research.

2 System Model

2.1 System model and channel assumptions

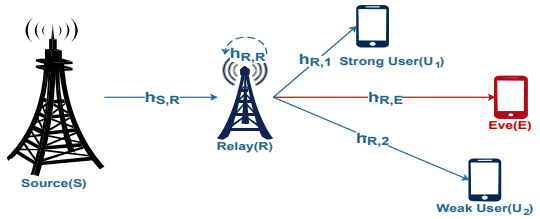

(a) NOMA FD system

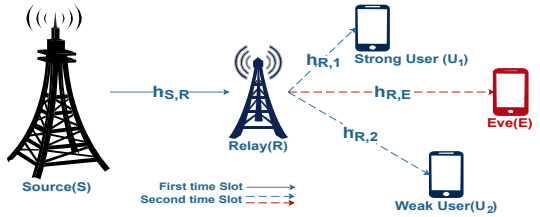

(b) NOMA HD system

Fig. 1 System Model

As shown in Fig. 1 , we consider a dual-hop NOMA system where a source (S) communicates with two NOMA users (U_1: strong user, U_2: weak user) through a relay (R) in the presence of one eavesdropper E . The relay works in AF/DF protocols in either half-duplex or full-duplex relaying mode. We assume that the S, U_1, U_2 and E are equipped with a single antenna while the relay facilitates two antennas, one for reception and one for transmission. Due to the deep fading between the source and users, as well as the eavesdropper, we assume that there is no direct link between them and reliable communication can only be supported via Relay-aid. We also assume that the transmission rate for each user is not larger than the corresponding achievable rate, which guarantees the successful decoding and successive interference cancelation at NOMA users. Here, we assume that all channels (from the source to the relay, from the relay to NOMA users, from the relay to the eavesdropper) are independent, identically distributed and modeled as $\kappa-\mu$ fading channels. We note that $\gamma_{a,b}=\frac{E_a}{N_b}|h_{a,b}|^2$ is the Signal-to-Noise-Ratio (SNR) of the $a-b$ link, E_a is the transmitted energy per symbol by a, N_b is the one-sided power spectral density of the additive white Gaussian noise (AWGN) at b and $h_{a,b}$ is the channel coefficient of the $a-b$ link.

2.2 Fading Model Assumptions

The $\kappa-\mu$ distribution is a general fading model that can be used to represent the small scale variation of the fading signal which is composed of clusters of multipath waves, each cluster has a dominant component letting this distribution well-suited for light-of-sight application. The parameter $\kappa\geq 0$ concerns the ratio between the total power of the dominant components and the total power of the scattered waves, whereas the parameter $\mu>0$ is related to the multipath clustering. According to Eq.2 [37], the probability density function (PDF: $f_{\gamma_{a,b}}(x)$) is given as

$$f_{\gamma_{a,b}}(x)=\frac{\mu(1+\kappa)^{\frac{\mu+1}{2}}}{\kappa^{\frac{\mu-1}{2}}exp(\mu\kappa)\tilde{\gamma}_{a,b}^{\frac{\mu+1}{2}}}x^{\frac{\mu-1}{2}}exp(-\frac{\mu(1+\kappa)}{\tilde{\gamma}_{a,b}}x) \\ I_{\mu-1}(2\mu\sqrt{\frac{\kappa(1+\kappa)}{\tilde{\gamma}_{a,b}}x}) \tag{1}$$

where $\tilde{\gamma}_{a,b}=\mathbb{E}(\gamma_{a,b})$ is the average SNR, $I_{\mu-1}(.)$ is the modified Bessel function of the first kind and $\mu-1$ order. Using the series expansion of the modified Bessel function of the first kind in [41] given as

$$I_v(z)=(\frac{1}{2}z)^v\sum_{r=0}^{\infty}\frac{(\frac{1}{4}z^2)^r}{r!\Gamma(r+v+1)} \tag{2}$$

Thus, the probability density function $f_{\gamma_{a,b}}(x)$ can be rewritten as

$$f_{\gamma_{a,b}}(x)=\frac{A_{a,b}^{\mu}}{exp(\mu\kappa)}exp(-A_{a,b}x)\sum_{r=0}^{\infty}\frac{x^{\mu+r-1}G^r}{r!\Gamma(r+\mu)} \tag{3}$$

where $A_{a,b}=\frac{\mu(1+\kappa)}{\tilde{\gamma}_{a,b}}$ and $G=\frac{\mu^2\kappa(1+\kappa)}{\tilde{\gamma}_{a,b}}$. The cumulative distribution function (CDF : $F_{\gamma_{a,b}}(x)$) of $\gamma_{a,b}$ can be obtained from Eq.3 in [37] as

$$F_{\gamma_{a,b}}(x)=1-Q_{\mu}\left[\sqrt{2\kappa\mu},\sqrt{\frac{2(1+\kappa)\mu x}{\tilde{\gamma}_{a,b}}}\right] \tag{4}$$

where $Q_{\mu}(.,.)$ is the generalized Marcum Q-function. We note that, the relay self-interference channel is assumed to undergo Rayleigh fading as in [38], which takes into account severe multipath fading conditions. Therefore, the PDF and CDF at the relay are, respectively, given as:

$$f_{\gamma_{R,R}}(x)=\frac{1}{\tilde{\gamma}_{R,R}}\exp(-\frac{x}{\tilde{\gamma}_{R,R}}) \tag{5}$$

$$F_{\gamma_{R,R}}(x)=\exp(-\frac{x}{\tilde{\gamma}_{R,R}}) \tag{6}$$

where $\tilde{\gamma}_{R,R}=\mathbb{E}(\gamma_{R,R})$.

2.3 Transmission Model Description

In this section, we describe the transmission process of the proposed network. During the block time t, the source transmits the superimposed signal to the relay. This signal is given by

$$s(t) = \sqrt{E_s}(\sqrt{\alpha_1}x_1(t) + \sqrt{\alpha_2}x_2(t)) \tag{7}$$

where x_i ($i \in \{1,2\}$) denotes the symbol for user U_i, E_s represents the transmit power of S and α_i is the attributed power allocation coefficient at the source of user i. To ensure users' quality of service, the power requirements must satisfy the following power constraints: $\alpha_1 < \alpha_2$ and $\alpha_1 + \alpha_2 = 1$.

Based on the aforementioned assumptions, during the t-th time slot, t= 1,2,3, ..., the received signal by the relay can be expressed as:

$$Y_R^{\eta}(t) = h_{S,R}s(t) + \zeta\sqrt{E_R}h_{R,R}s(t) + N_R(t) \tag{8}$$

where $\eta = \{HD, FD\}$ is the relay mode, $h_{S,R}$ is the channel coefficient between the S and R. $h_{R,R}$ denotes the loop-back interference channel from the transmit antenna to the receive antenna at the relay. ζ is the state factor between HD and FD mode with $\zeta = 0$ and $\zeta = 1$ denote the relay R working in HD and FD mode, respectively. As in [14], we assume that the delay time, in FD mode, for the signal processing is small compared to the block time t. Therefore, it is ignored in our analysis. We also assume that the residual self-interference channel (SI) relay $\rightarrow$ relay is modeled as a Gaussian random variable with zero mean and variance $\lambda_{R,R} = \omega\mathbb{E}(|h_{R,R}|^2)$ [14, 15], the parameter ω is the level of the residual self-interference at R. we note that $\gamma_{R,R} = \frac{E_R}{N_R}|h_{R,R}|^2$ is the instantaneous received SNR at the SI link.

2.3.1 Decode-and-Forward Relaying

Applying NOMA, the DF relay decodes its received superimposed message from the source in the first phase using SIC. First, x_1 is treated as noise to decode x_2, and then we cancel the interference caused by x_2 to acquire x_1 from Eq(8). Therefore, the the signal-to-interference-ratio (SINR) at the relay R to detect x_1 and x_2 are given by

$$\gamma_{R,x_2}^{\eta,DF} = \frac{\alpha_2\gamma_{S,R}}{\alpha_1\gamma_{S,R} + \zeta\gamma_{R,R} + 1} = \frac{\alpha_2\gamma_R^{\eta}}{\alpha_1\gamma_R^{\eta} + 1} \tag{9}$$

$$\gamma_{R,x_1}^{\eta,DF} = \frac{\alpha_1\gamma_{S,R}}{\zeta\gamma_{R,R} + 1} = \alpha_1\gamma_R^{\eta} \tag{10}$$

where $\gamma_R^{\eta} = \frac{\gamma_{S,R}}{\zeta\gamma_{R,R}+1}$ is the SINR of the first hope. Then, the decoded message is sent to NOMA users. Due to the broadcast nature of wireless transmissions, E also receives a copy of the signal. Therefore, the received signals at U_1, U_2 and E are given by

$$Y_j^{DF}(t) = h_{R,j}\sqrt{E_R}\sum_{i=1}^{2}\sqrt{\beta_i}x_i(t) + N_j(t) \tag{11}$$

where $j \in \{1,2,E\}$, $h_{R,j}$ is the channel coefficients between R and destinations U_1,U_2 and E, β_i is the power allocation coefficient at the relay of user i with $\beta_1 + \beta_2 = 1$ and N_j is the AWGN at the destinations. Based on Eq(11), the SINR of x_2 observed at the strong user is given by

$$\gamma_{1\rightarrow 2}^{DF} = \frac{\beta_2\gamma_{R,1}}{\beta_1\gamma_{R,1} + 1} \tag{12}$$

We assume that the achievable rate of the weak users' signal at the strong user exceeds the target data rate of the weak user. So, the strong user can successfully decode the weak user's message and can perform a perfect SIC to remove weak user signal. Therefore, the signal-to-noise ratio (SNR) at U_1 is given as

$$\gamma_{R1}^{DF} = \beta_1\gamma_{R,1} \tag{13}$$

On the other hand, by treating the signal x_1 as co-channel interference, the SINR of x_2 at the weak user can be given by

$$\gamma_{R2}^{DF} = \frac{\beta_2\gamma_{R,2}}{\beta_1\gamma_{R,2} + 1} \tag{14}$$

It is noted that for the DF relay system, the end-to-end SINR of the system at U_1 and U_2 is respectively defined as

$$\gamma_1^{\eta,DF} = min(\gamma_{R,x_1}^{\eta,DF}, \gamma_{R1}^{DF}) \tag{15}$$

$$\gamma_2^{\eta,DF} = min(\gamma_{R,x_2}^{\eta,DF}, \gamma_{R2}^{DF}) \tag{16}$$

For the wiretapping scenario, we assume the worst case, each eavesdropper has multiuser detection ability by using Parallel Interference Cancellation (PIC) technique to distinguish the superimposed mixture of NOMA user's signal. Therefore, the SINR to wiretap the signal of the legitimate NOMA user U_i in HD/FD mode is given by

$$\gamma_{E\rightarrow i}^{\eta,DF} = \beta_i\gamma_{R,E} \tag{17}$$

2.3.2 Amplify-and-Forward Relaying

In this scenario, the relay broadcasts its received signal in Eq(8) after amplifying it. Therefore, the received signal at destinations U_1, U_2 and E can be expressed as

$$\begin{aligned} Y_j^{\eta,AF}(t) &= Gh_{R,j}Y_R^{\eta}(t) + N_j(t) \\ &= \underbrace{Gh_{R,j}h_{S,R}\sqrt{E_s\alpha_1}x_1(t)}_{Desired\ Signal\ for\ U_1} + \underbrace{Gh_{R,j}h_{S,R}\sqrt{E_s\alpha_2}x_2(t)}_{Desired\ Signal\ for\ U_2} \\ &+ \underbrace{Gh_{R,j}\zeta h_{R,R}\sqrt{E_R}s(t)}_{Self-Interference\ signal} + \underbrace{Gh_{R,j}N_R(t) + N_j(t)}_{Noise\ signal} \end{aligned} \tag{18}$$

where $j \in \{1,2,E\}$ and G is the relaying gain calculated as [13, 17]

$$G = \sqrt{\frac{E_R}{E_s|h_{S,R}|^2 + \zeta E_R|h_{R,R}|^2 + N_R}} \tag{19}$$

With the assumption of perfect successive interference cancellation, the strong user U_1 first subtracts the signal of the weak user U_2: x_2 through SIC. Therefore, the equivalent SINR $\gamma_{1\to 2}$ is expressed as

$$\gamma_{1\to 2}^{\eta,AF} = \frac{\alpha_2\, G^2 E_s|h_{S,R}|^2|h_{R,1}|^2}{\alpha_1\, G^2 E_s|h_{S,R}|^2|h_{R,1}|^2 + \zeta G^2|h_{R,1}|^2 E_R|h_{R,R}|^2 + G^2|h_{R,1}|^2 N_R + N_1} \tag{20}$$

After some mathematical manipulations, $\gamma_{1\to 2}$ can be simplified as follow

$$\gamma_{1\to 2}^{\eta,AF} = \frac{\alpha_2\gamma_{S,R}\gamma_{R,1}}{\alpha_1\gamma_{S,R}\gamma_{R,1} + \gamma_{R,1}\zeta\gamma_{R,R} + \gamma_{S,R} + \gamma_{R,1} + \zeta\gamma_{R,R} + 1} \tag{21}$$

By considering $\gamma_R^{\eta} = \frac{\gamma_{S,R}}{\zeta\gamma_{R,R}+1}$ as the SINR at the first hope, $\gamma_{1\to 2}$ is rewritten as

$$\gamma_{1\to 2}^{\eta,AF} = \frac{\alpha_2\gamma_R^{\eta}\gamma_{R,1}}{\alpha_1\gamma_R^{\eta}\gamma_{R,1} + \gamma_R^{\eta} + \gamma_{R,1} + 1} \tag{22}$$

Then, U_1 decodes its own symbol x_1 and its SINR can be calculated as

$$\gamma_1^{\eta,AF} = \frac{\alpha_1\gamma_{S,R}\gamma_{R,1}}{\zeta\gamma_{R,R}\gamma_{R,1} + \gamma_{S,R} + \gamma_{R,1} + \zeta\gamma_{R,R} + 1} = \frac{\alpha_1\gamma_R^{\eta}\gamma_{R,1}}{\gamma_R^{\eta} + \gamma_{R,1} + 1} \tag{23}$$

The SINR at U_2 can be written as

$$\begin{aligned}\gamma_2^{\eta,AF} &= \frac{\alpha_2\gamma_{S,R}\gamma_{R,2}}{\alpha_1\gamma_{S,R}\gamma_{R,2} + \gamma_{R,2}\zeta\gamma_{R,R} + \gamma_{S,R} + \gamma_{R,2} + \zeta\gamma_{R,R} + 1} \\ &= \frac{\alpha_2\gamma_R^{\eta}\gamma_{R,2}}{\alpha_1\gamma_R^{\eta}\gamma_{R,2} + \gamma_R^{\eta} + \gamma_{R,2} + 1}\end{aligned} \tag{24}$$

Using PIC, E try to decode users signals. Thus, the equivalent SINR at E is given by

$$\begin{aligned}\gamma_{E\to i}^{\eta,AF} &= \frac{\alpha_i\gamma_{S,R}\gamma_{R,E}}{\zeta\gamma_{R,R}\gamma_{R,E} + \gamma_{R,E} + \gamma_{S,R} + \zeta\gamma_{R,R} + 1} \\ &= \frac{\alpha_i\gamma_R^{\eta}\gamma_{R,E}}{\gamma_R^{\eta} + \gamma_{R,E} + 1}\end{aligned} \tag{25}$$

where $i \in \{1,2\}$.

2.4 Secrecy Capacity Expression

The secrecy capacity is defined as the maximum rate of a communication within the information can be decoded reliably at the legitimate receiver but not at the eavesdropper. The secrecy capacity in HD/FD AF/DF NOMA systems can be expressed as

$$Sc_i^{\eta,\Delta} = \left(\frac{1}{2}\right)^{1-\zeta}[log_2(1+\gamma_i^{\eta,\Delta}) - log_2(1+\gamma_{E\to i}^{\eta,\Delta})]^+ \tag{26}$$

Where $\Delta \in \{AF, DF\}$.

3 Secrecy Outage Probability

In this section, we will investigate the secrecy level of the NOMA system in terms of secrecy outage probability when channels undergoes $\kappa-\mu$ fading. A secrecy outage occurs when the secrecy capacity Sc is less than a predefined threshold R_s for a particular fading distribution. It can be formulated in the NOMA system as [33, 34]

$$\begin{aligned}SOP^{\eta,\Delta} &= \mathbb{P}\left(Sc_1^{\eta,\Delta} < R_{s1}\ or\ Sc_2^{\eta,\Delta} < R_{s2}\right) \\ &= 1 - \mathbb{P}\left(Sc_1^{\eta,\Delta} > R_{s1}\right) \times \mathbb{P}\left(Sc_2^{\eta,\Delta} > R_{s2}\right) \\ &= 1 - \left(1 - SOP_{U_1}^{\eta,\Delta}\right) \times \left(1 - SOP_{U_2}^{\eta,\Delta}\right)\end{aligned} \tag{27}$$

where $SOP_{U_1}^{\eta,\Delta}$ and $SOP_{U_2}^{\eta,\Delta}$ are the SOP for user 1 and 2, respectively.

3.1 SOP analysis for U_1

At the strong user, the SOP can be expressed as

$$SOP_{U_1}^{\eta,\Delta} = \mathbb{P}(Sc_1^{\eta,\Delta} < R_1) = \mathbb{P}\left(\frac{1+\gamma_1^{\eta,\Delta}}{1+\gamma_{E\to 1}^{\eta,\Delta}} < C_1^{\eta}\right) \tag{28}$$

where $C_1^{\eta} = 2^{2^{1-\zeta}R_{s_1}}$.

Case1: C-NOMA based DF relaying: The SOP of U_1 is given as

$$\begin{aligned} SOP_{U_1}^{\eta,DF} =& \mathbb{P}\left(\frac{1+\gamma_1^{\eta,DF}}{1+\gamma_{E\to1}^{\eta,DF}} < C_1^{\eta}\right) \\ =& \mathbb{P}(min(\alpha_1\gamma_R^{\eta},\beta_1\gamma_{R,1}) < C_1^{\eta}\beta_1\gamma_{R,E} + C_1^{\eta} - 1) \\ =& 1 - \underbrace{\mathbb{P}(\gamma_R^{\eta} > \theta_1^{\eta}\gamma_{R,E} + \theta_2^{\eta})}_{\Phi_1^{\eta,DF}} \times \underbrace{\mathbb{P}(\gamma_{R,1} > C_1^{\eta}\gamma_{R,E} + \theta_3^{\eta})}_{\Phi_2^{\eta,DF}} \end{aligned} \tag{29}$$

where $\theta_1^{\eta} = \frac{C_1^{\eta}\beta_1}{\alpha_1}$, $\theta_2^{\eta} = \frac{C_1^{\eta}-1}{\alpha_1}$. $\theta_3^{\eta} = \frac{C_1^{\eta}-1}{\beta_1}$.

Case2: C-NOMA based AF relaying: We opt for an upper bound of the strong user and the eavesdropper SINR due to the intractable nature of the SOP expression: $\gamma_1^{\eta,AF} = \frac{\alpha_1\gamma_R^{\eta}\gamma_{R,1}}{\gamma_R^{\eta}+\gamma_{R,1}+1} \approx \frac{\alpha_1\gamma_R^{\eta}\gamma_{R,1}}{\gamma_R^{\eta}+\gamma_{R,1}}$ and $\gamma_{E\to1}^{\eta,AF} = \frac{\alpha_1\gamma_R^{\eta}\gamma_{R,E}}{\gamma_R^{\eta}+\gamma_{R,E}+1} \approx \frac{\alpha_1\gamma_R^{\eta}\gamma_{R,E}}{\gamma_R^{\eta}+\gamma_{R,E}}$. From [17], $\gamma_1^{\eta,AF}$ can be rewritten as $\gamma_1^{\eta,AF} = \alpha_1 min(\gamma_R^{\eta},\gamma_{R,1})$ and $\gamma_{E\to1}^{\eta,AF} = \alpha_1 min(\gamma_R^{\eta},\gamma_{R,E})$. Therefore, Eq(28) can be expressed in AF case as

$$\begin{aligned} SOP_{U_1}^{\eta,AF} =& \mathbb{P}\left(\frac{1+\alpha_1 min(\gamma_R^{\eta},\gamma_{R,1})}{1+\alpha_1 min(\gamma_R^{\eta},\gamma_{R,E})} < C_1^{\eta}\right) \\ =& \mathbb{P}\left(min(\gamma_R^{\eta},\gamma_{R,1}) < C_1^{\eta} min(\gamma_R^{\eta},\gamma_{R,E}) + \theta_2^{\eta}\right) \\ \approx& \mathbb{P}\left(min(\gamma_R^{\eta},\gamma_{R,1}) < C_1^{\eta}\gamma_{R,E} + \theta_2^{\eta}\right) \\ =& 1 - \underbrace{\mathbb{P}\left(\gamma_R^{\eta} > C_1^{\eta}\gamma_{R,E} + \theta_2^{\eta}\right)}_{\Phi_1^{\eta,AF}} \times \underbrace{\mathbb{P}\left(\gamma_{R,1} > C_1^{\eta}\gamma_{R,E} + \theta_2^{\eta}\right)}_{\Phi_2^{\eta,AF}} \end{aligned} \tag{30}$$

Proposition 1: The secrecy outage probability at U_1 can be determined for both AF and DF protocols using FD and HD mode as follows

$$\begin{aligned} SOP_{U_1}^{\eta,\Delta} =& 1 - \mathbb{P}\left(\gamma_R^{\eta} > X^{\eta,\Delta}\gamma_{R,E} + \theta_2^{\eta}\right) \times \mathbb{P}\left(\gamma_{R,1} > C_1^{\eta}\gamma_{R,E} + Y^{\eta,\Delta}\right) \\ =& 1 - \Phi_1^{\eta,\Delta} \times \Phi_2^{\eta,\Delta} \end{aligned} \tag{31}$$

Where $X^{\eta,DF} = \theta_1^{\eta}$, $Y^{\eta,DF} = \theta_3^{\eta}$, $X^{\eta,AF} = C_1^{\eta}$ and $Y^{\eta,AF} = \theta_2^{\eta}$.

3.1.1 Full-duplex analysis

We begin by calculation $\Phi_1^{FD,\Delta}$ as

$$\Phi_1^{FD,\Delta} = \int_0^{\infty}(1 - F_{\gamma_R^{FD}}(X^{FD,\Delta}x + \theta_2^{FD,\Delta}))f_{\gamma_{R,E}}(x)dx \tag{32}$$

First, $F_{\gamma_R^{FD}}(x)$ is given as

$$F_{\gamma_R^{FD}}(x) = 1 - \frac{e^{-\kappa\mu}}{\tilde{\gamma}_{R,R}}\sum_{n=0}^{\infty}\frac{(\kappa\mu)^n}{n!}\sum_{m=0}^{n+\mu-1}\sum_{p=0}^{m}\frac{A_{S,R}^m e^{-A_{S,R}x}x^m}{(m-p)!(\frac{1}{\tilde{\gamma}_{R,R}} + A_{S,R}x)^{p+1}} \tag{33}$$

where κ,μ are the fading coefficients at legitimate receivers and $A_{S,R} = \frac{(1+\kappa)\mu}{\tilde{\gamma}_{S,R}}$.

(Proof see Appendix A)

Then, $\Phi_1^{FD,\Delta}$ is given as

$$\begin{aligned} \Phi_1^{FD,\Delta} =& \frac{A_{R,E}^{\mu_e}e^{-\kappa\mu-\kappa_e\mu_e-A_{S,R}\theta_2^{FD,\Delta}}}{\tilde{\gamma}_{R,R}}\sum_{n=0}^{\infty}\frac{(\kappa\mu)^n}{n!}\sum_{m=0}^{n+\mu-1}\sum_{p=0}^{m}\frac{A_{S,R}^{m-(p+1)}}{(m-p)!} \\ & \sum_{q=0}^{m}\binom{m}{q}(\theta_2^{FD,\Delta})^{m-q}(X^{FD,\Delta})^{q-(p+1)}\sum_{r=0}^{\infty}\frac{G_e^r}{r!}(D_1^{FD,\Delta})^{t-(p+1)} \\ & \Gamma\left[\begin{matrix} t \\ r+\mu_e \end{matrix}\right]\mathbf{U}(t,t-p;D_1^{FD,\Delta}\times B_1^{FD,\Delta}) \end{aligned} \tag{34}$$

(Proof: see Appendix B)

where $t = q + r + \mu_e$ and $\mathbf{U}(.,.,.)$ is the Kummer function known as the degenerate hypergeometric function of one variable defined by

$$\mathbf{U}(a,b;x) = \frac{1}{\Gamma(a)}\int_0^{\infty} exp(-xt)t^{a-1}(1+t)^{b-a-1}dt \tag{35}$$

Secondly, $\Phi_2^{FD,\Delta}$ can be obtained as

$$\begin{aligned} \Phi_2^{FD,\Delta} =& A_{R,E}^{\mu_e}e^{-\kappa\mu-\kappa_e\mu_e-A_{R,1}Y^{FD,\Delta}}\sum_{n=0}^{\infty}\frac{(\kappa\mu)^n}{n!}\sum_{m=0}^{n+\mu-1}A_{R,1}^m \\ & \sum_{p=0}^{m}\frac{(C_1^{FD})^p(Y^{FD,\Delta})^{m-p}}{p!(m-p)!(B_2^{FD})^{(p+\mu_e)}}\Gamma\left[\begin{matrix} p+\mu_e \\ \mu_e \end{matrix}\right]{}_1F_1\left(p+\mu_e,\mu_e,\frac{G_e}{B_2^{FD}}\right) \end{aligned} \tag{36}$$

(Proof: see Appendix C)

3.1.2 Half-duplex analysis

We note when $\eta = HD$, we have $\zeta = 0$. Thus, $\gamma_R^{HD} = \gamma_{S,R}$ and Φ_1^{HD} can be expressed as

$$\Phi_1^{HD,\Delta} = \int_0^{\infty}(1 - F_{\gamma_{S,R}}(X^{HD,\Delta}x + \theta_2^{HD}))f_{\gamma_{R,E}}(x)dx \tag{37}$$

Using the same analysis to obtain Eq(36), $\Phi_1^{HD,\Delta}$ is given as

$$\begin{aligned} \Phi_1^{HD,\Delta} =& A_{R,E}^{\mu_e}e^{-\kappa\mu-\kappa_e\mu_e-A_{S,R}\theta_2^{HD}}\sum_{n=0}^{\infty}\frac{(\kappa\mu)^n}{n!}\sum_{m=0}^{n+\mu-1}\sum_{p=0}^{m}\frac{A_{S,R}^m(X^{HD,\Delta})^p}{p!(m-p)!} \\ & (\theta_2^{HD})^{m-p}(B_1^{HD,\Delta})^{-(p+\mu_e)}\Gamma\left[\begin{matrix} p+\mu_e \\ \mu_e \end{matrix}\right]{}_1F_1\left(p+\mu_e,\mu_e,\frac{G_e}{B_1^{HD,\Delta}}\right) \end{aligned} \tag{38}$$

Where $B_1^{HD,\Delta}=A_{R,E}+A_{S,R}X^{HD,\Delta}$. Likely, Φ_2^{HD} is obtained as

$$\Phi_2^{HD}=A_{R,E}^{\mu_e}e^{-\kappa\mu-\kappa_e\mu_e-A_{R,1}Y^{HD,\Delta}}\sum_{n=0}^{\infty}\frac{(\kappa\mu)^n}{n!}\sum_{m=0}^{n+\mu-1}\sum_{p=0}^{m}\frac{A_{R,1}^m(C_1^{HD})^p}{p!(m-p)!}(Y^{HD,\Delta})^{m-p}(B_2^{HD})^{-(p+\mu_e)}\Gamma\begin{bmatrix}p+\mu_e\\ \mu_e\end{bmatrix}{}_1F_1\left(p+\mu_e,\mu_e,\frac{G_e}{B_2^{HD}}\right) \tag{39}$$

where $B_2^{HD}=A_{R,E}+A_{R,1}C_1^{HD}$.

3.2 SOP analysis for U_2

Due to the intractable nature of U_2 SINR for both AF and DF relaying scenario, we focus at the analysis on high SNR region.

3.2.1 C-NOMA based DF relaying

An upper bound for the SINR of U_2 can be obtain as $\gamma_2^{\eta,DF}=min(\frac{\alpha_2\gamma_R^\eta}{\alpha_1\gamma_R^\eta+1},\frac{\beta_2\gamma_{R,2}}{\beta_1\gamma_{R,2}+1})\approx min(\frac{\alpha_2}{\alpha_1},\frac{\beta_2}{\beta_1})$. Then, the SOP of the weak user is expressed as

$$\begin{aligned}SOP_{U_2}^{\eta,DF}=&\mathbb{P}(\frac{1+\gamma_2^{\eta,DF}}{1+\gamma_{E\to2}^{\eta,DF}}<C_2^\eta)\\=&\mathbb{P}(\frac{1+min(\frac{\alpha_2}{\alpha_1},\frac{\beta_2}{\beta_1})}{1+\beta_2\gamma_{R,E}}<C_2^\eta)\\=&\mathbb{P}(\gamma_{R,E}>\frac{min(\frac{\alpha_2}{\alpha_1},\frac{\beta_2}{\beta_1})+1-C_2^\eta}{\beta_2C_2^\eta})\\=&1-F_{\gamma_{R,E}}(\theta_4^{\eta,DF})\end{aligned} \tag{40}$$

where $C_2^\eta=2^{2^{1-\zeta}R_2}$ and $\theta_4^{\eta,DF}=\frac{min(\frac{\alpha_2}{\alpha_1},\frac{\beta_2}{\beta_1})+1-C_2^\eta}{\beta_2C_2^\eta}$. Therefore, the SOP of U_2 using FD/HD relaying mode is obtained as

$$SOP_{U_2}^{\eta,DF}=Q_{\mu_e}\left(\sqrt{2\kappa_e\mu_e},\sqrt{2A_{R,E}\theta_4^{\eta,DF}}\right) \tag{41}$$

3.2.2 C-NOMA based AF relaying

For the weak user U_2, an upper bound for the SINR of U_2 can be obtain as $\gamma_2^{\eta,AF}\approx\frac{\alpha_2}{\alpha_1}$ and $\gamma_{E\to2}^{\eta,AF}=\alpha_2min(\gamma_R^\eta,\gamma_{R,E})$. Then, the SOP of the weak user is expressed as

$$\begin{aligned}SOP_{U_2}^{\eta,AF}=&\mathbb{P}(Sc_2^{\eta,AF}<R_2)\\=&\mathbb{P}\left(\frac{1+\gamma_2^{\eta,AF}}{1+\gamma_{E\to2}^{\eta,AF}}<2^{2^{1-\zeta}R_2}\right)\\=&\mathbb{P}(\frac{1}{\alpha_1}<C_2^\eta+C_2^\eta\gamma_{E\to2}^{\eta,AF})\\=&\mathbb{P}(min(\gamma_R^\eta,\gamma_{R,E})>\frac{1-\alpha_1C_2^\eta}{\alpha_1\alpha_2C_2^\eta})\\=&(1-F_{\gamma_R^\eta}(\theta_4^{\eta,AF}))\times(1-F_{\gamma_{R,E}}(\theta_4^{\eta,AF}))\end{aligned} \tag{42}$$

where $\theta_4^{\eta,AF}=\frac{1-\alpha_1C_2^\eta}{\alpha_1\alpha_2C_2^\eta}$.

Full-duplex analysis:

$$SOP_{U_2}^{FD,AF}=\frac{e^{-\kappa\mu-A_{S,R}\theta_4^{FD,AF}}}{\tilde{\gamma}_{R,R}}\sum_{n=0}^{\infty}\frac{(\kappa\mu)^n}{n!}\sum_{m=0}^{n+\mu-1}\sum_{p=0}^{m}\frac{A_{S,R}^m(\theta_4^{FD,AF})^m}{(m-p)!}\frac{Q_{\mu_e}\left(\sqrt{2\kappa_e\mu_e},\sqrt{2A_{R,E}\theta_4^{FD,AF}}\right)}{(\frac{1}{\tilde{\gamma}_{R,R}}+A_{S,R}\theta_4^{FD,AF})^{p+1}} \tag{43}$$

Half-duplex analysis:

$$\begin{aligned}SOP_{U_2}^{HD,AF}=&Q_\mu\left(\sqrt{2\kappa\mu},\sqrt{2A_{S,R}\theta_4^{FD,AF}}\right)\\&\times Q_{\mu_e}\left(\sqrt{2\kappa_e\mu_e},\sqrt{2A_{R,E}\theta_4^{FD,AF}}\right)\end{aligned} \tag{44}$$

4 Strictly Positive Secrecy Capacity (SPSC)

In the following we derive closed form expressions of the Strictly Positive Secrecy Capacity Probability to get more insight on the existence of secrecy capacity. The SPSC in NOMA system can be given by

$$\begin{aligned}SPSC^{\eta,\Delta}=&\mathbb{P}(Sc_1^{\eta,\Delta}>0\,,\,SC_2^{\eta,\Delta}>0)\\=&\mathbb{P}(Sc_1^{\eta,\Delta}>0)\times\mathbb{P}(Sc_2^{\eta,\Delta}>0)\\=&SPSC_{U_1}^{\eta,\Delta}\times SPSC_{U_2}^{\eta,\Delta}\end{aligned} \tag{45}$$

where $SPSC_{U_1}^{\eta,\Delta}$ and $SPSC_{U_2}^{\eta,\Delta}$ are the SPSC for user 1 and user 2, respectively.

4.1 SPSC at U_1

C-NOMA based DF relaying In this case, we calculate the SPSC of U_1 as

$$\begin{aligned}SPSC_{U_1}^{\eta,DF}=&\mathbb{P}(Sc_1^{\eta,DF}>0)\\=&\mathbb{P}(min(\alpha_1\gamma_R^\eta,\beta_1\gamma_{R,1})>\beta_1\gamma_{R,E})\\=&\underbrace{\mathbb{P}(\gamma_R^\eta>Z^{DF}\gamma_{R,E})}_{\Phi_3^{\eta,DF}}\times\underbrace{\mathbb{P}(\gamma_{R,1}>\gamma_{R,E})}_{\Phi_4^{\eta,DF}}\end{aligned} \tag{46}$$

where $Z^{DF}=\frac{\beta_1}{\alpha_1}$.

C-NOMA based AF relaying We calculate the SPSC of U_1 as

$$\begin{aligned}SPSC_{U_1}^{\eta,AF}=&\mathbb{P}(Sc_1^{\eta,AF}>0)\\=&\mathbb{P}(min(\gamma_R^\eta,\gamma_{R,1})>min(\gamma_R^\eta,\gamma_{R,E}))\\\approx&1-\mathbb{P}(min(\gamma_R^\eta,\gamma_{R,1})<\gamma_{R,E})\\=&\underbrace{\mathbb{P}(\gamma_R^\eta>\gamma_{R,E})}_{\Phi_3^{\eta,AF}}\times\underbrace{\mathbb{P}(\gamma_{R,1}>\gamma_{R,E})}_{\Phi_4^{\eta,AF}}\end{aligned} \tag{47}$$

Proposition 2: The strictly positive secrecy capacity at U_1 can be obtained for both AF/DF relaying in FD/HD mode as

$$SPSC_{U_1}^{\eta,\Delta} = \underbrace{\mathbb{P}(\gamma_R^{\eta} > Z^{AF}\gamma_{R,E})}_{\Phi_3^{\eta,\Delta}} \times \underbrace{\mathbb{P}(\gamma_{R,1} > \gamma_{R,E})}_{\Phi_4^{\eta,\Delta}} \tag{48}$$

where $Z^{AF} = 1$.

4.1.1 Full-duplex analysis

First, we calculate $\Phi_3^{FD,\Delta}$ as

$$\Phi_3^{FD,\Delta} = \int_0^{\infty} (1 - F_{\gamma_R^{\eta}}(Z^{\Delta}x)) f_{\gamma_{R,E}}(x)dx \tag{49}$$

Using Eq(33) and Eq(3) in Eq(49), $\Phi_3^{FD,\Delta}$ will be written as

$$\begin{aligned}\Phi_3^{FD,\Delta} = &\frac{A_{R,E}^{\mu_e} e^{-\kappa\mu-\kappa_e\mu_e}}{\tilde{\gamma}_{R,R}} \sum_{n=0}^{\infty} \frac{(\kappa\mu)^n}{n!} \sum_{m=0}^{n+\mu-1} \sum_{p=0}^{m} \frac{(Z^{\Delta}A_{S,R})^{m-(p+1)}}{(m-p)!} \\ &\sum_{r=0}^{\infty} \frac{G_e^r}{r!\Gamma(r+\mu_e)} \int_0^{\infty} \frac{x^{m+r+\mu_e-1}\exp(-(Z^{\Delta}A_{S,R}+A_{R,E})x)}{(\frac{1}{Z^{\Delta}A_{S,R}\tilde{\gamma}_{R,R}}+x)^{p+1}}dx\end{aligned} \tag{50}$$

Using Eq(2.3.6.9) in [42], we can solve Eq(50) integral as

$$\begin{aligned}\Phi_3^{FD,\Delta} = &A_{R,E}^{\mu_e} e^{-\kappa\mu-\kappa_e\mu_e} \sum_{n=0}^{\infty} \frac{(\kappa\mu)^n}{n!} \sum_{m=0}^{n+\mu-1} \sum_{p=0}^{m} \sum_{r=0}^{\infty} \frac{G_e^r (Z^{\Delta}A_{S,R})^{-(r+\mu_e)}}{(m-p)!r!\tilde{\gamma}_{R,R}^{m+r+\mu_e-p}} \\ &\Gamma\begin{bmatrix} m+r+\mu_e \\ r+\mu_e \end{bmatrix} \mathbf{U}(m+r+\mu_e, m+r+\mu_e-p; \frac{Z^{\Delta}A_{S,R}+A_{R,E}}{Z^{\Delta}A_{S,R}\tilde{\gamma}_{R,R}})\end{aligned} \tag{51}$$

Secondly, $\Phi_4^{FD,\Delta}$ can be expressed as

$$\Phi_4^{FD,\Delta} = \int_0^{\infty} (1 - F_{\gamma_{R,1}}(x)) f_{\gamma_{R,E}}(x)dx \tag{52}$$

Using the same analysis to solve Eq(36) integral, $\Phi_4^{FD,\Delta}$ is given as

$$\begin{aligned}\Phi_4^{FD,\Delta} = &A_{R,E}^{\mu_e} e^{-\kappa\mu-\mu_e\kappa_e} \sum_{n=0}^{\infty} \frac{(\kappa\mu)^n}{n!} \sum_{m=0}^{n+\mu-1} \frac{A_{R,1}^m (A_{R,1}+A_{R,E})^{-(m+\mu_e)}}{m!} \\ &\Gamma\begin{bmatrix} m+\mu_e \\ \mu_e \end{bmatrix} {}_1F_1\left(m+\mu_e, \mu_e, \frac{G_e}{A_{R,1}+A_{R,E}}\right)\end{aligned} \tag{53}$$

4.1.2 Half-duplex analysis

Using the same analysis to obtain $\Phi_4^{HD,\Delta}$, $\Phi_3^{HD,\Delta}$ is given as

$$\begin{aligned}\Phi_3^{HD,\Delta} = &A_{R,E}^{\mu_e} e^{-\kappa\mu-\mu_e\kappa_e} \sum_{n=0}^{\infty} \frac{(\kappa\mu)^n}{n!} \sum_{m=0}^{n+\mu-1} \frac{(Z^{\Delta}A_{S,R})^m}{m!(Z^{\Delta}A_{S,R}+A_{R,E})^{m+\mu_e}} \\ &\Gamma\begin{bmatrix} m+\mu_e \\ \mu_e \end{bmatrix} {}_1F_1\left(m+\mu_e, \mu_e, \frac{G_e}{Z^{\Delta}A_{S,R}+A_{R,E}}\right)\end{aligned} \tag{54}$$

From Eq(47) and Eq(48), we can notice that $\Phi_4^{HD,\Delta} = \Phi_4^{FD,\Delta}$, therefore, $\Phi_4^{HD,\Delta}$ is obtained as in Eq(53).

4.2 SPSC at U_2

4.2.1 C-NOMA based AF relaying

The SPSC of U_2 is expressed as

$$\begin{aligned}SPSC_{U_2}^{\eta,AF} = &\mathbb{P}(Sc_2^{\eta,AF} > 0) = \mathbb{P}(\frac{\alpha_2}{\alpha_1} > \alpha_2 min(\gamma_R^{\eta},,\gamma_{R,E})) \\ = &1 - \mathbb{P}(\gamma_R^{\eta} > \frac{1}{\alpha_1}) \times \mathbb{P}(\gamma_{R,E} > \frac{1}{\alpha_1}) \\ = &1 - (1 - F_{\gamma_R^{\eta}}(\frac{1}{\alpha_1})) \times (1 - F_{\gamma_{R,E}}(\frac{1}{\alpha_1}))\end{aligned} \tag{55}$$

Full-duplex analysis Using Eq(33) and Eq(4), the SPSC at U_2 in FD mode is given as

$$\begin{aligned}SPSC_{U_2}^{FD,AF} = &1 - \frac{e^{-\kappa\mu-\frac{A_{S,R}}{\alpha_1}}}{\tilde{\gamma}_{R,R}} \sum_{n=0}^{\infty} \frac{(\kappa\mu)^n}{n!} \sum_{m=0}^{n+\mu-1} \sum_{p=0}^{m} \frac{A_{S,R}^m \alpha_1^{-m}}{(m-p)!} \\ &\times \frac{Q_{\mu_e}\left(\sqrt{2\kappa_e\mu_e}, \sqrt{\frac{2A_{R,E}}{\alpha_1}}\right)}{(\frac{1}{\tilde{\gamma}_{R,R}} + \frac{A_{S,R}}{\alpha_1})^{p+1}}\end{aligned} \tag{56}$$

Half-duplex analysis: Using Eq(4), the SPSC at U_2 in HD mode is given as

$$\begin{aligned}SPSC_{U_2}^{HD,AF} = &1 - Q_{\mu}\left(\sqrt{2\kappa\mu}, \sqrt{\frac{2A_{S,R}}{\alpha_1}}\right) \\ &\times Q_{\mu_e}\left(\sqrt{2\kappa_e\mu_e}, \sqrt{\frac{2A_{R,E}}{\alpha_1}}\right)\end{aligned} \tag{57}$$

4.2.2 C-NOMA based DF relaying

The SPSC of U_2 is expressed as

$$\begin{aligned}SPSC_{U_2}^{\eta,DF} &= \mathbb{P}(Sc_2^{\eta,DF} > 0) \\ &= \mathbb{P}(min(\frac{\alpha_2}{\alpha_1}, \frac{\beta_2}{\beta_1}) > \beta_2\gamma_{R,E}) \\ &= F_{\gamma_E}(\theta_5)\end{aligned} \tag{58}$$

where $\theta_5 = \frac{min(\frac{\alpha_2}{\alpha_1}, \frac{\beta_2}{\beta_1})}{\beta_2}$. For both FD and HD mode, the SPSC at U_2 is obtained by

$$SPSC_{U_2}^{\eta,DF} = 1 - Q_{\mu_e}\left(\sqrt{2\kappa_e\mu_e}, \sqrt{2A_{R,E}\theta_5}\right) \tag{59}$$

5 Numerical Results

In this section, numerical results are presented to illustrate the effect of fading, average and eavesdropper SNR, data rate and the transmit power allocation factor on the system secrecy outage and capacity performance. Monte Carlo simulations are provided and carried out through 10^7 iterations, to validate the proposed analytical results. In all the figures below, 'Ana' and 'Sim' denotes, respectively, the analytical and simulation results. Unless otherwise stated, all numerical results plotted in this section will adopt the following set-up:

- The transmit power at the source is equal to the transmit power at the relay; $E_s = E_R = E$.
- The noise at legitimate receivers is equal where $N_R = N_1 = N_2 = N_0$.
- N_E is the noise at the eavesdropper.

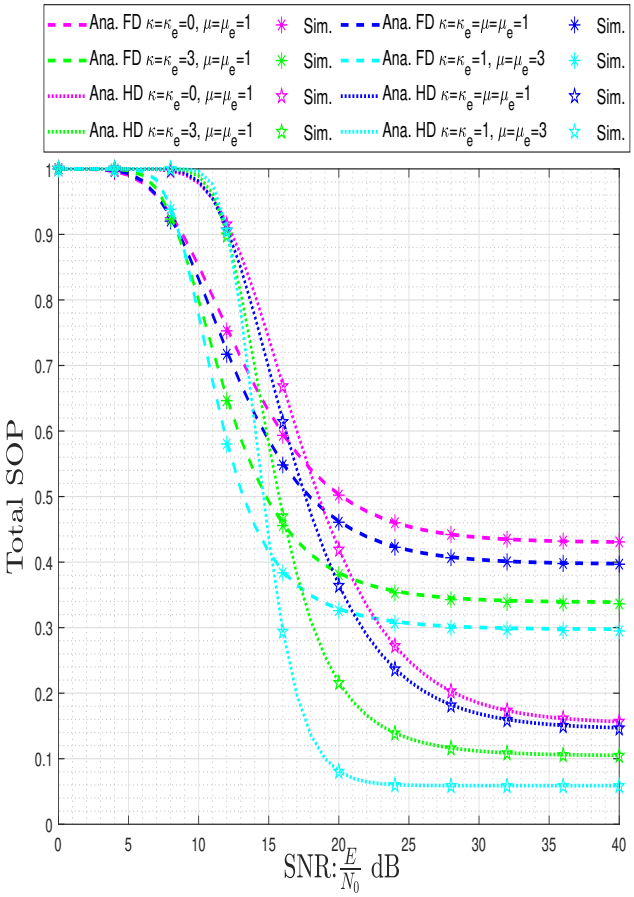

Fig. 2 Total SOP of NOMA system with Full/Half Duplex DF relaying versus different SNR values: $\alpha_2 = \beta_2 = 0.8$, $R_{s1} = 1$ Bit Per Channel Use (BPCU), $R_{s2} = 0.5$ BPCU, $\frac{E}{N_e} = 0$ dB.

Figures 2 and 3 detail the system secrecy outage probability for AF/DF relaying in half and full duplex mode with different SNR ($\frac{E}{N_0}$) and fading parameters values (κ, κ_e, μ and μ_e). From the figures, it can be seen that the secrey outage decreases as the SNR becomes high. We also note that FD-based NOMA system achieves superior secrecy at low-medium SNR. Otherwise, the HD mode performs better at high SNR, which can be explained by the effect of self-interference at the FD relay that increases as the noise increases. In addition, different combinations of the fading parameters for the legitimate κ, μ and eavesdropper channels κ_e, μ_e are considered. The results show that the increase in fading parameters at both legitimate κ, μ and eavesdropper node κ_e, μ_e causes the reduction in the secrecy outage probability. It can be seen that when channels suffer from severe multipath fading modeled by Rayleigh fading ($\kappa = \kappa_e = 0, \mu = \mu_e = 1$) the worse the system secrecy becomes. Moreover, we can observe that when the light-of-sight (LoS) become stronger ($\kappa = \kappa_e = 3$), the system secrecy gets ameliorated and grows significantly faster with the increase in the number of multipath clusters ($\mu = \mu_e = 3$). We note that the exact analytical results match precisely with the simulations, which demonstrates the correctness of our analysis.

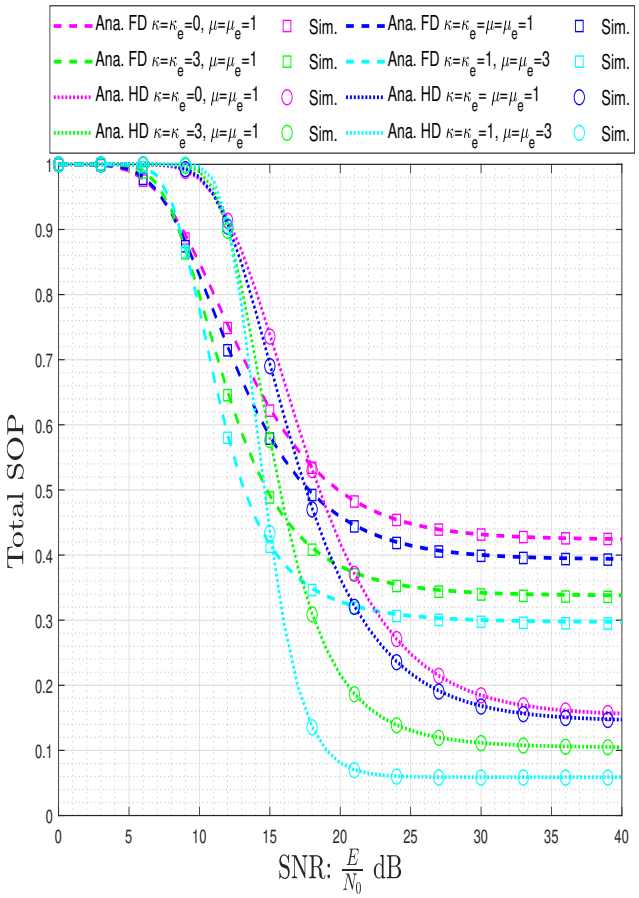

Fig. 3 Total SOP of NOMA system with Full/Half Duplex AF relaying versus different SNR values: $\alpha_2 = \beta_2 = 0.8$, $R_{s1} = 1$ BPCU, $R_{s2} = 0.5$ BPCU, $\frac{E}{N_e} = 0$ dB.

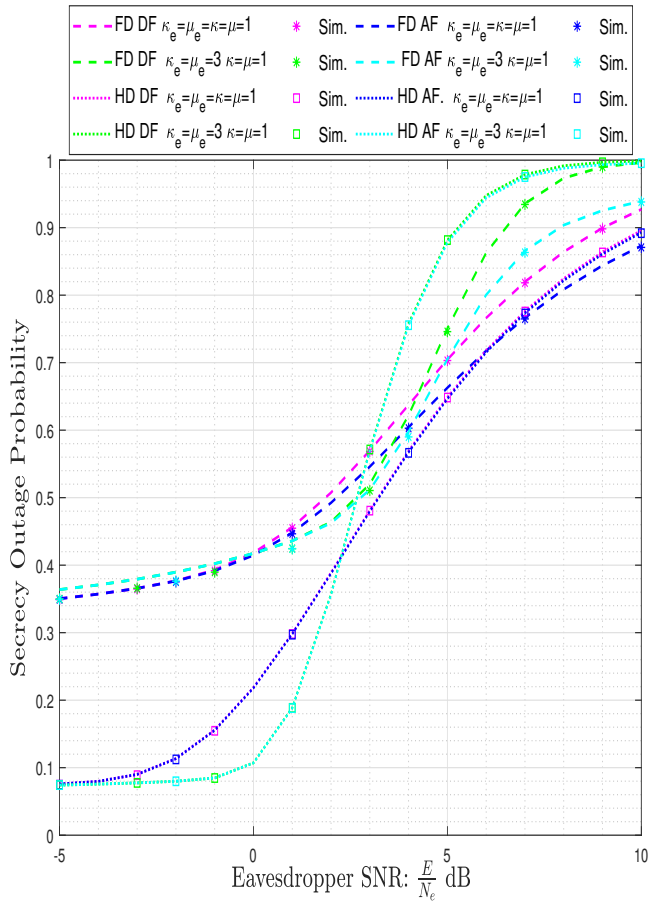

Fig. 4 The SOP of AF/DF NOMA system with Full/Half Duplex relaying versus different eavesdropper SNR values: $\alpha_2 = \beta_2 = 0.8$, $R_{s1} = 1$ BPCU, $R_{s2} = 0.5$ BPCU, $\frac{E}{N_0} = 25$ dB.

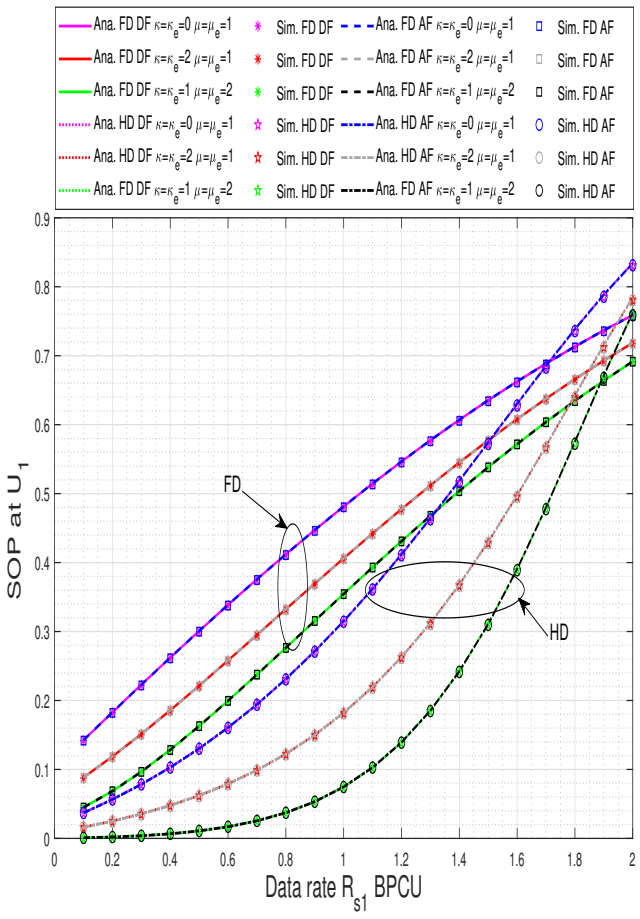

Fig. 5 The SOP of AF/DF NOMA system with Full/Half Duplex relaying versus different secrecy data rate values: $\alpha_2 = \beta_2 = 0.8$, $\frac{E}{N_0} = 20$ dB and $\frac{E}{N_e} = 0$ dB.

Figure 4 illustrates the effect of the eavesdropper SNR on the SOP of FD/HD AF/DF NOMA system where different combinations of the fading parameters of the eavesdropper channel $\kappa_e = \mu_e = 1$ and $\kappa_e = \mu_e = 3$ were considered. It can be seen that the NOMA system secrecy is deteriorated as the eavesdropper SNR increases. We also notice that with the increase of the fading parameters of the eavesdropper channel, the HD relaying performs better for low eavesdropper SNR ($<\approx$ 3dB), otherwise, the FD relay grants better secrecy and more secrecy is achieved when using AF protocol.

Figures 5 and 6 depict the effect of NOMA users secrecy rate R_{s1} and R_{s2} on the behaviours of the SOP of user U_1 and U_2 for different fading parameters where $\kappa = \kappa_e \in \{0,1,2\}$ and $\mu = \mu_e \in \{1,2\}$. It is observed that the secrecy performance at each user decreases as the data rate increases. In other words, better secrecy is achieved when low secrecy rate are attributed to both strong and weak NOMA users. It is also noted that the FD relay offer better secrecy than HD relay for weak user U_2 and also for strong user U_1 when high data rates are used. The effect of fading is also demonstrated in these figures, we can notice a remarkable improvement on the secrecy of the strong NOMA user when the fading parameters increase. Obviously, it can be seen that the secrecy performance of the weak user degrades when the fading severity decreases and the data rate exceeds > 0.7 and > 1.4 for HD and FD relaying, respectively.

Figure 7 illustrates the total secrecy outage of the NOMA system as a function of the average SNR for different secrecy data rates. As, it was shown in Fig. 5 and Fig. 6, when high secrecy data rates are used: $R_{s1} = 2$ and $R_{s2} = 1$, better secrecy performance is obtained by the FD NOMA system. Although, when we decrease the data rate for both NOMA users, we note that HD relaying outperforms FD for high SNR $\frac{E}{N_0} > 15$.

Figure 8 investigates the behaviour of the SOP of FD/HD AF protocol for both strong and weak NOMA users U_1 and U_2 as a function of the attributed power coefficient for U_1; α_1. We can remark that the secrecy outage decreases as the power coefficient increases for the strong user. Or, in the concept of NOMA more power is granted to the weak user

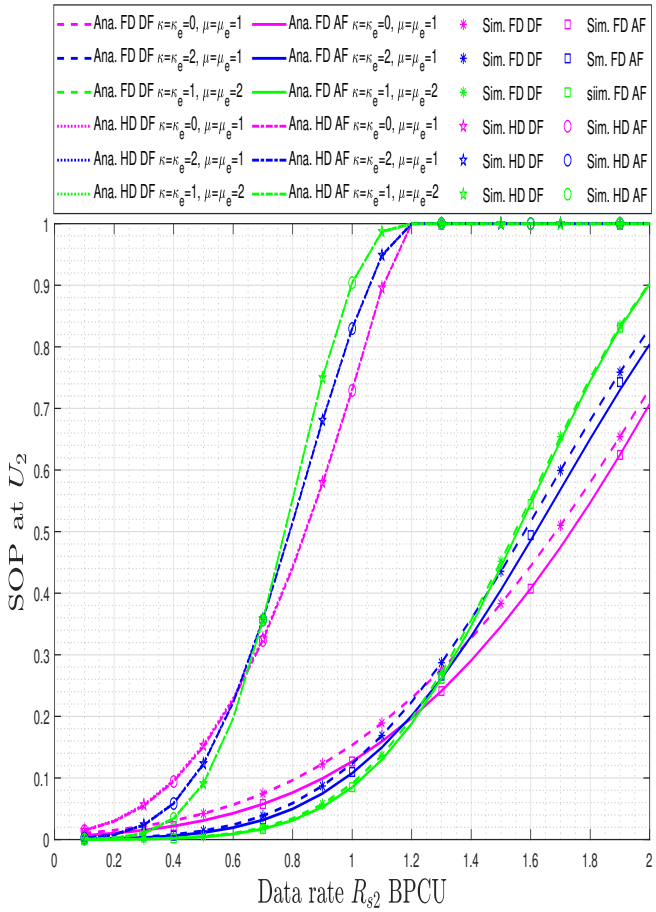

Fig. 6 The SOP of AF/DF NOMA system with Full/Half Duplex relaying versus different secrecy data rate values: $\alpha_2=\beta_2=0.8$, $\frac{E}{N_0}=20$ dB and $\frac{E}{N_e}=0$ dB.

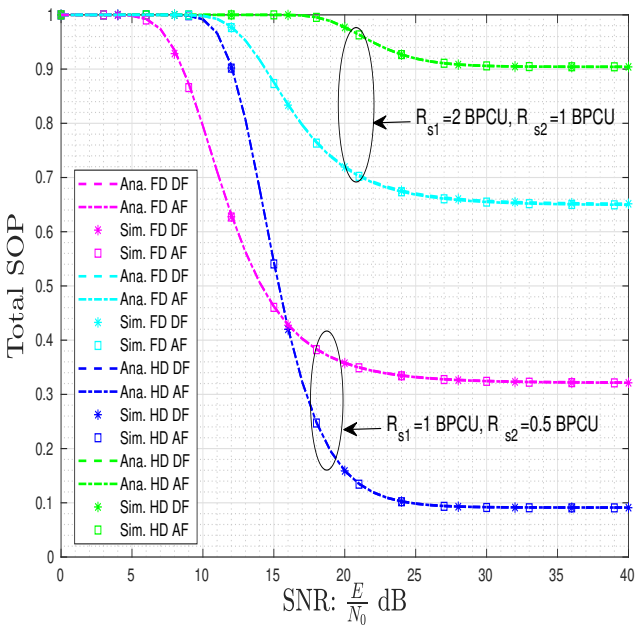

Fig. 7 SOP of AF/DF NOMA system with Full/Half Duplex relaying versus different SNR values: $\alpha_2=\beta_2=0.8$, $\frac{E}{N_e}=0$ dB, $\kappa_e=\mu_e=1$, $\kappa=0$, $\mu=2$.

which clearly affects the secrecy of the strong user and grants more secrecy for the weak user. It is also shown that FD relaying grants better secrecy than HD for weak NOMA user. Alternatively, increasing fading parameters improves the secrecy of the strong user, otherwise, for the weak user high fading parameters affects better the secrecy when high power coefficient is affect to the strong user.

Figure 9 shows the performance of the SOP of both U_1 and U_2 using FD DF protocol as a function of the power attributed to the strong user at the relay; β_1. We can note that with increasing power coefficient values of U_1 at the source α_1, the secrecy gets ameliorated for the strong user and significantly detiorated for the weak user. It is also observed that the SOP of U_1 and U_2 gets increased as the power coeffecient at the the relay β_1 increases, approximatly for $\beta_1 > \approx 0.1$ for U_1 and $\beta_1 > \approx \alpha_1$ for U_2. We can also remark that the increase of fading parameters improves the secrecy of the strong user and slightly deteriorate the secrcey of the weak user.

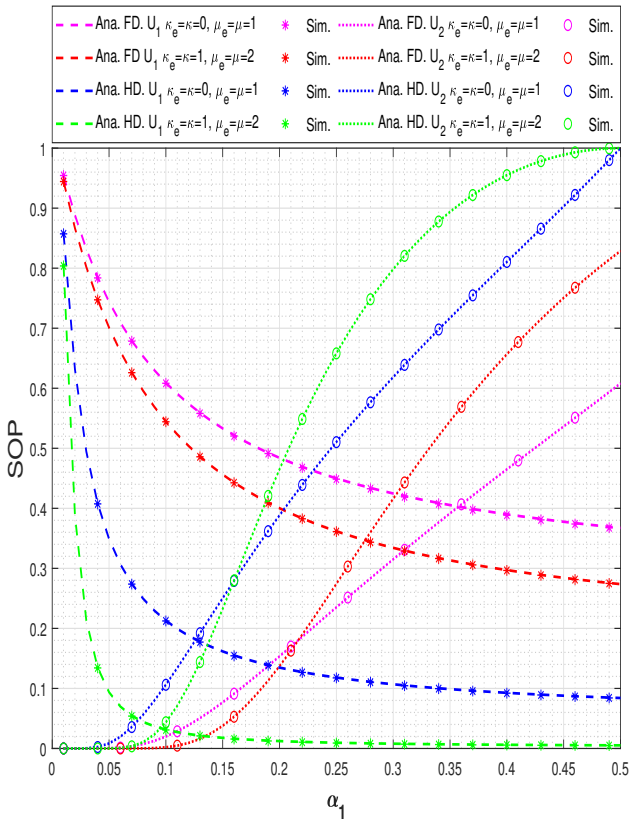

Fig. 8 The SOP of AF NOMA system with Full/Half Duplex relaying versus different allocaed power values: $R_{s1}=1$, $R_{s2}=0.5$, $\frac{E}{N_0}=25$ dB, $\frac{E}{N_e}=3$ dB.

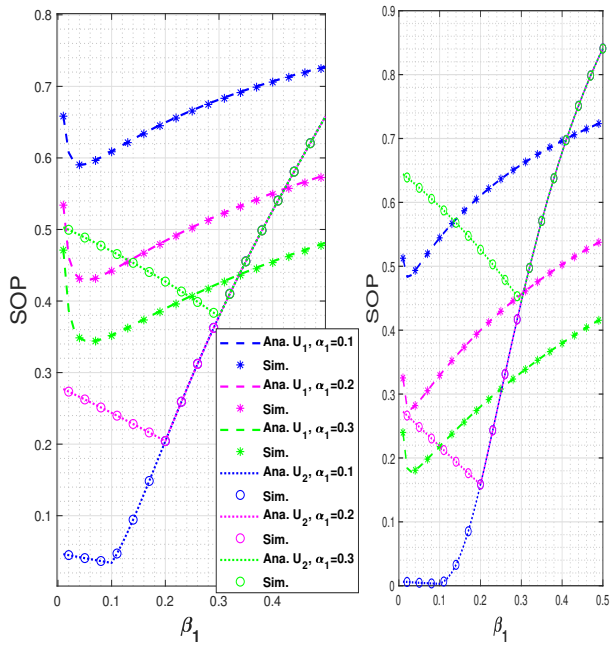

(a) Rayleigh Fading (b) $\kappa_e = \kappa = 1$, $\mu_e = \mu = 2$

Fig. 9 SOP of DF NOMA system with Full-Duplex relaying versus different β_1 values: $R_{s1} = 1BPCU$, $R_{s2} = 0.5$ BPCU, $\frac{E}{N_0} = 25$ dB, $\frac{E}{N_e} =$ 3 dB.

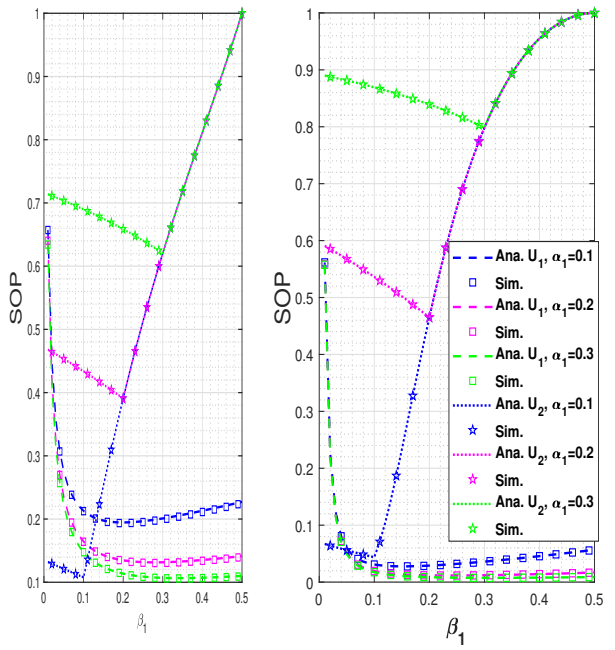

(a) Rayleigh Fading (b) $\kappa_e = \kappa = 1$, $\mu_e = \mu = 2$

Fig. 10 SOP of DF NOMA system with Half-Duplex relaying versus different β_1 values: $R_{s1} = 1BPCU$, $R_{s2} = 0.5$ BPCU, $\frac{E}{N_0} = 25$ dB, $\frac{E}{N_e} =$ 3 dB.

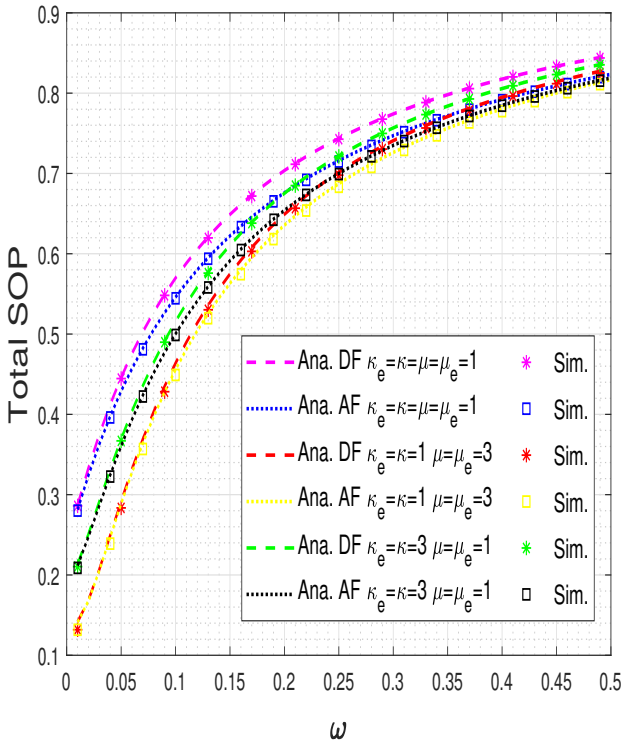

Fig. 11 SOP of Full-Duplex AF/DF NOMA system relaying versus different values of the self-interference parameter ω : $\alpha_2 = \beta_2 = 0.8$, $\frac{E}{N_e} = 3$ dB, $\frac{E}{N_0} = 25$ dB.

Figure 10 details the performance of the SOP using HD DF protocol with the same parameters as in Fig. 9. It is clearly shown that the increase of the source power coefficient of the strong user α_1 ameliorates the secrecy of the strong user and profoundly deteriorates the secrecy of the weak user. It is also observed that the increase of the power coefficients at the the relay β_1 slightly deteriorates the secrecy of U_1 and remarkably deteriorates the secrecy of U_2 when $\beta_1 >\approx \alpha_1$. Furthermore, we note that the increase of the fading coefficients slightly influences on the SOP of the strong user but continue to reduce the secrecy of the weak user.

From Figures 8, 9 and 10, we can notice the existence of a secrecy gap between strong and weak users related to the concept of NOMA which attributes low power coefficient to the strong user.

Figure 11 investigates the effect the self-interference parameter ω on the secrecy outage probability. It clearly shows that the increase of the self interference profoundly deteriorates the secrecy of the FD NOMA system. Besides, the SOP decreases as the fading coefficients increase almost remarkably when the self interference is low. As the value of ω increases, the DF relaying outperforms the AF relaying. This is because in the AF relaying scheme, the received self-interference noise is amplified and forwarded with the sig-

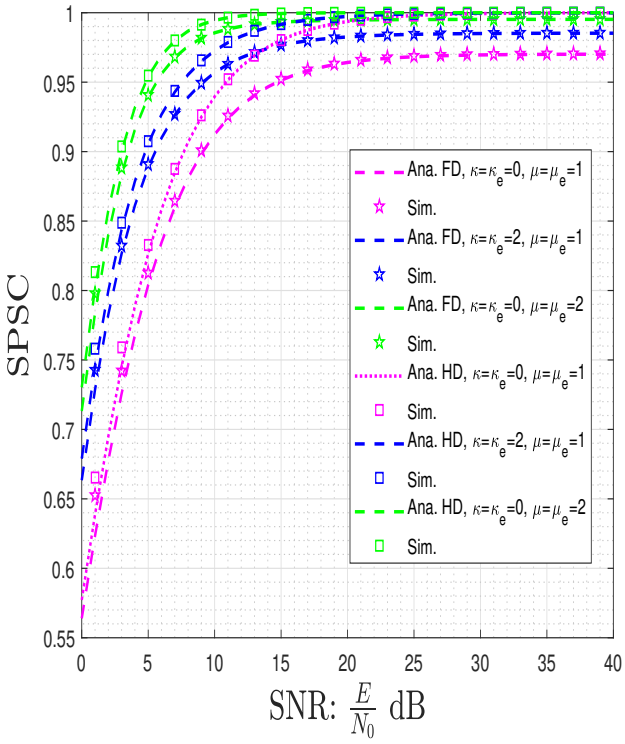

Fig. 12 The SPSC of FD/HD AF NOMA system versus different SNR values: $\alpha_2=\beta_2=0.8$, $\frac{E}{N_0}=25$ dB, $\frac{E}{N_e}=-5$ dB.

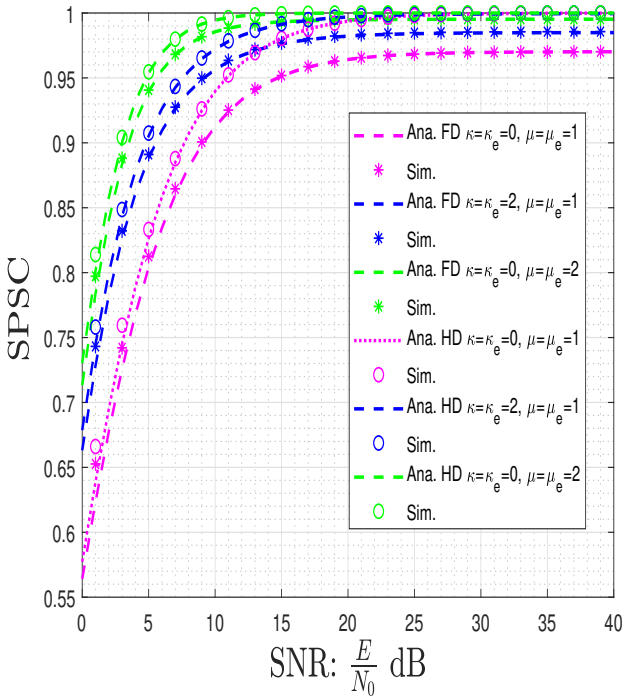

Fig. 13 The SOP of FD/HD DF NOMA system versus different SNR values: $\alpha_2=\beta_2=0.8$, $\frac{E}{N_0}=25$ dB, $\frac{E}{N_e}=-5$ dB.

nal. We also note that the increase in multipath clusters μ,μ_e grants more secrecy than the increase in the light of sight components κ,κ_e.

Figures 12 and 13 illustrate the strictly positive secrecy capacity of both AF/DF NOMA systems using FD and HD relaying for different values of fading and average SNR. We can observe that the secrecy capacity of AF/DF NOMA system increases with the increase of the average transmitted SNR and fading parameters. We can also notice that, in this case, the HD NOMA system allows more secrecy capacity than the FD NOMA system.

Figures 14 and 15 show the effect of the eavesdropper SNR on the SPSC of FD/HD AF and DF relaying with different power coefficients at the DF relay; β. It is observed that the eavesdropper SNR increases, the secrecy capacity diminishs. We also notice as the DF relay power coefficient increases, its non-zero secrecy capacity increases. Thus, we concluse that when the relay power coefficient β_2 is superior than the source power coefficient α_2, the DF relaying barely outperforms AF relaying using FD mode and low eavesdropper SNR $\frac{E}{N_e}<5$ dB. Otherwise, AF relaying grants more secrecy capacity.

6 Conclusions

In this paper, we presented a physical layer security study of Full-Duplex / Half-Duplex Amplify-and-Forward / Decode-and-Forward relaying based NOMA system over $\kappa-\mu$ fading channels. The secrecy outage probability and the strictly positive secrecy capacity were derived for both strong and weak NOMA users with simple mathematically tractable closed-form expressions. From the obtained results, we infer that fading can ameliorate the secrecy of NOMA system when the eavesdropper SNR is low and the increase in multipath clusters has more positive secrecy impact than the increase in the light-of-sight components. Otherwise, when the eavesdropper SNR is high, having high fading detriorates more the secrecy performance. Moreover, we deduce that FD relaying gives more secrecy to the weak user, unlike HD relaying which gears more secrecy to the strong user. We also note that there is a huge security gap between NOMA users and this is mainly due to the power sharing concept linked to NOMA which results in a security unfairness between the weak and the strong NOMA users. Finally, we note on one hand that AF relaying grants more secrecy for high average and eavesdropper SNR scenerios and on the other hand, the DF relaying performs better in the FD scenario when the self-interference is high.

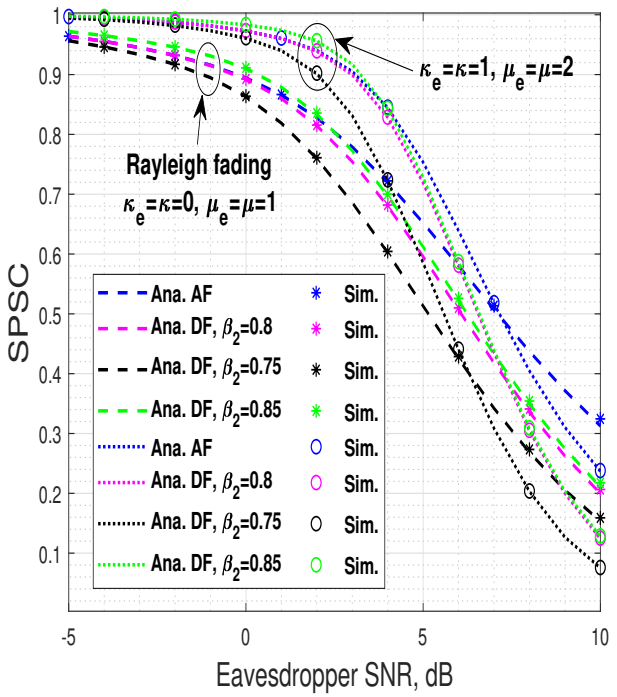

Fig. 14 The SPSC of FD AF/DF NOMA system versus different values of the eavesdropper SNR: $\alpha_2 = 0.8$, $\frac{E}{N_0} = 25$ dB.

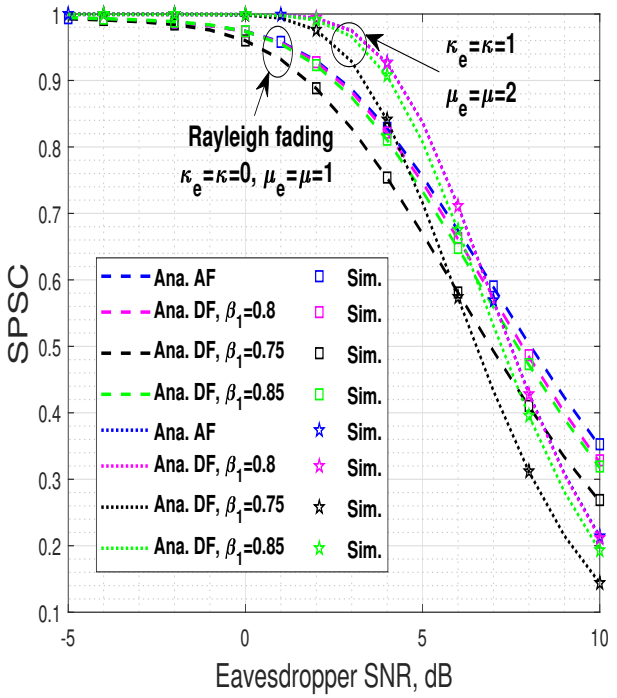

Fig. 15 The SPSC of HD AF/DF NOMA system versus different values of the eavesdropper SNR: $\alpha_2 = 0.8$, $\frac{E}{N_0} = 25$ dB.

Declarations

- Authors' contributions : It is the contribution of PHD student Nesrine Zaghdoud, Pr Adel Ben Mnaouer, Pr Hatem Boujemaa and Pr Farid Touati.
- Funding : Publication supported by Canadian University of Dubai.
- Conflicts of interest/Competing interests : The authors state that there is no conflict of interest for this paper.
- Availability of data and material : Material and data are not available.

A Proof of Equation (33)

In FD mode, We remind that $\zeta = 1$. Therefore, the CDF of γ_R^{FD} can be expressed as

$$\begin{aligned} F_{\gamma_R^{FD}}(x) =& \mathbb{P}(\frac{\gamma_{S,R}}{\gamma_{R,R}+1} < x) = 1 - \mathbb{P}(\gamma_{S,R} > x(1+\gamma_{R,R})) \\ =& 1 - \int_0^{\infty} (1 - F_{\gamma_{S,R}}(x(1+y))) f_{\gamma_{R,R}}(y) dy \\ =& 1 - \int_0^{\infty} Q_{\mu}(\sqrt{2\kappa\mu}, \sqrt{\frac{2(1+\kappa)\mu x(1+y)}{\tilde{\gamma}_{S,R}}}) \\ & \times \frac{1}{\tilde{\gamma}_{R,R}} exp(-\frac{y}{\tilde{\gamma}_{R,R}}) dy \end{aligned} \tag{60}$$

Through the definition of the Marcum Q function in Eq 4.47 [39], $F_{\gamma_R^{FD}}(x)$ will be written as

$$\begin{aligned} F_{\gamma_R^{FD}}(x) = 1 - \frac{1}{\tilde{\gamma}_{R,R}} \sum_{n=0}^{\infty} exp(-\kappa\mu) \frac{(\kappa\mu)^n}{n!} \sum_{m=0}^{n+\mu-1} exp(-\frac{(1+\kappa)\mu}{\tilde{\gamma}_{S,R}} x) \\ (\frac{(1+\kappa)\mu}{\tilde{\gamma}_{S,R}})^m \frac{x^m}{m!} \int_0^{\infty} (1+y)^m exp(-(\frac{1}{\tilde{\gamma}_{R,R}} + \frac{(1+\kappa)\mu}{\tilde{\gamma}_{S,R}} x) y) dy \end{aligned} \tag{61}$$

Using the defintion of the power series expansion in Eq(1.111) and Eq(3.381.4) [40] to solve the integral, Eq(61) can be solved as in Eq(33).

B Proof of Equation (34)

Using Eq(33) and Eq(3) in Eq(32), $\Phi_1^{FD,\Delta}$ can be expressed as

$$\begin{aligned} \Phi_1^{FD,\Delta} = & \int_0^{\infty} \frac{1}{\tilde{\gamma}_{R,R}} \sum_{n=0}^{\infty} exp(-\kappa\mu) \frac{(\kappa\mu)^n}{n!} \\ & \sum_{m=0}^{n+\mu-1} \sum_{p=0}^{m} \frac{A_{S,R}^m (X^{\eta,\Delta} x + \theta_2^{\eta,\Delta})^m \exp(-A_{S,R}(X^{\eta,\Delta} x + \theta_2^{\eta,\Delta}))}{(m-p)! (\frac{1}{\tilde{\gamma}_{R,R}} + A_{S,R}(X^{FD,\Delta} x + \theta_2^{FD,\Delta}))^{p+1}} \\ & \times \frac{A_{R,E}^{\mu_e}}{exp(\mu_e \kappa_e)} exp(-A_{R,E} x) \sum_{r=0}^{\infty} \frac{x^{r+\mu_e-1} G_e^r}{r! \Gamma(r+\mu_e)} dx \end{aligned} \tag{62}$$

where κ_e, μ_e are the fading coefficient at the eavedropper, $A_{R,E} = \frac{\mu_e(1+\kappa_e)}{\tilde{\gamma}_{R,E}}$ and $G_e = \frac{\mu_e^2 \kappa_e (1+\kappa_e)}{\tilde{\gamma}_{R,E}}$. Using Eq(1.111) [40], Eq(62) can be rewritten as

$$\Phi_1^{FD,\Delta} = \frac{A_{R,E}^{\mu_e} e^{-\kappa_e\mu_e - A_{S,R}\theta_2^{\eta,\Delta}}}{\tilde{\gamma}_{R,R}} \sum_{n=0}^{\infty} \exp(-\kappa\mu)\frac{(\kappa\mu)^n}{n!} \sum_{m=0}^{n+\mu-1} \sum_{p=0}^{m} \frac{A_{S,R}^{m-(p+1)}}{(m-p)!} \sum_{q=0}^{m} \binom{m}{q} (\theta_2^{FD,\Delta})^{m-q} (X^{FD,\Delta})^{q-(p+1)} \sum_{r=0}^{\infty} \frac{G_e^r}{r!\Gamma(\mu_e+r)} \int_0^{\infty} \frac{x^{r+q+\mu_e-1}\exp(-B_1^{FD}x)}{(D_1^{FD,\Delta}+x)^{p+1}} dx \quad (63)$$

Where $B_1^{FD,\Delta} = A_{R,E} + A_{S,R}X^{FD,\Delta}$, $D_1^{FD,\Delta} = \frac{1}{\tilde{\gamma}_{R,R}A_{S,R}X^{FD,\Delta}} + \frac{\theta_2^{FD,\Delta}}{X^{FD,\Delta}}$. Using Eq(2.3.6.9) in [42], we can solve Eq(63) integral as in Eq(34).

C Proof of Equation (36)

From Eq(31), $\Phi_2^{FD,\Delta}$ can be expressed as

$$\Phi_2^{FD,\Delta} = \int_0^{\infty} (1 - F_{\gamma_{R,1}}(C_1^{FD}x + \theta_1^{FD}))f_{\gamma_{R,E}}(x)dx \quad (64)$$

Using the series expansion of the marcum Q function in Eq(4.47) [38] and the definition of the power series in Eq(1.111) [41], $\Phi_2^{FD,\Delta}$ can be expressed as

$$\Phi_2^{FD,\Delta} = \frac{\mu_e(1+\kappa_e)^{\frac{\mu_e+1}{2}}}{\kappa_e^{\frac{\mu_e-1}{2}} exp(\mu_e\kappa_e)\tilde{\gamma}_{R,E}^{\frac{\mu_e+1}{2}}} exp(-A_{R,1}\theta_1^{FD}) \sum_{n=0}^{\infty} exp(-\kappa\mu)\frac{(\kappa\mu)^n}{n!} \sum_{m=0}^{n+\mu-1} \sum_{p=0}^{m} \frac{A_{R,1}^m (C_1^{FD})^p}{p!(m-p)!} (Y^{FD,\Delta})^{m-p} \int_0^{\infty} x^{p+\frac{\mu_e-1}{2}} exp(-B_2^{FD}x) I_{\mu_e-1}(2\mu_e\sqrt{\frac{\kappa_e(1+\kappa_e)}{\tilde{\gamma}_{R,E}}x})dx \quad (65)$$

where $B_2^{FD} = A_{R,E} + A_{R,1}C_1^{FD}$ and $A_{R,1} = \frac{(1+\kappa)\mu}{\tilde{\gamma}_{R,1}}$. Let t = $\sqrt{x}$, dx = 2tdt. By using Eq.2.15.5.4 [43] , we can rewrite last equation integral as

$$\int_0^{\infty} 2t^{2p+\mu_e} exp(-B_2^{FD}t^2) I_{\mu_e-1}(2\mu_e\sqrt{\frac{\kappa_e(1+\kappa_e)}{\tilde{\gamma}_{R,E}}}t)dt = \left(\mu_e\sqrt{\frac{\kappa_e(1+\kappa_e)}{\tilde{\gamma}_{R,E}}}\right)^{\mu_e-1} (B_2^{FD})^{-(p+\mu_e)}\Gamma\begin{bmatrix} p+\mu_e \\ \mu_e \end{bmatrix} {}_1F_1\left(p+\mu_e, \mu_e, \frac{G_e}{B_2^{FD}}\right) \quad (66)$$

where ${}_1F_1$ is the Gauss hypergeometric function, as defined by Eq(9.100) in [43].

References

1. Vaezi, M., Ding, Z., & Poor, H. V. (Eds.). (2019). Multiple access techniques for 5G wireless networks and beyond. Berlin, Germany: Springer.
2. Dai, L., Wang, B., Ding, Z., Wang, Z., Chen, S., & Hanzo, L. (2018). A survey of non-orthogonal multiple access for 5G. IEEE communications surveys & tutorials, 20(3), 2294-2323.
3. Liu, Y., Qin, Z., & Ding, Z. (2020). Non-Orthogonal Multiple Access for Massive Connectivity. Springer.
4. Higuchi, K., & Benjebbour, A. (2015). Non-orthogonal multiple access (NOMA) with successive interference cancellation for future radio access. IEICE Transactions on Communications, 98(3), 403-414.
5. Meng, L., Su, X., Zhang, X., Choi, C., & Choi, D. (2018). Signal reception for successive interference cancellation in NOMA downlink. Proceedings of the 2018 Conference on Research in Adaptive and Convergent Systems, https://doi.org/10.1145/3264746.3264751.
6. Ding, Z., Peng, M., & Poor, H. V. (2015). Cooperative non-orthogonal multiple access in 5G systems. IEEE Communications Letters, 19(8), 1462-1465.
7. Liaqat, M., Noordin, K. A., Latef, T. A., & Dimyati, K. (2020). Power-domain non orthogonal multiple access (PD-NOMA) in cooperative networks: an overview. Wireless Networks, 26(1), 181-203.
8. Fitzek, F. H., & Katz, M. D. (2006). Cooperation in wireless networks: principles and applications (421-461). New York: Springer.
9. Boujema, H. (2011). Static hybrid amplify and forward (AF) and decode and forward (DF) relaying for cooperative systems. Physical Communication, 4(3), 196-205.
10. Kim, J. B., & Lee, I. H. (2015). Capacity analysis of cooperative relaying systems using non-orthogonal multiple access. IEEE Communications Letters, 19(11), 1949-1952.
11. Liang, X., Wu, Y., Ng, D. W. K., Zuo, Y., Jin, S., & Zhu, H. (2017). Outage performance for cooperative NOMA transmission with an AF relay. IEEE Communications Letters, 21(11), 2428-2431.
12. Yang, Z., Ding, Z., Wu, Y., & Fan, P. (2017). Novel relay selection strategies for cooperative NOMA. IEEE Transactions on Vehicular Technology, 66(11), 10114-10123.
13. Men, J., Ge, J., & Zhang, C. (2016). Performance analysis of nonorthogonal multiple access for relaying networks over Nakagami-*m* fading channels. IEEE Transactions on Vehicular Technology, 66(2), 1200-1208.
14. Zhong, C., & Zhang, Z. (2016). Non-orthogonal multiple access with cooperative full-duplex relaying. IEEE Communications Letters, 20(12), 2478-2481.
15. Chu, T. M. C., & Zepernick, H. J. (2018). Performance of a non-orthogonal multiple access system with full-duplex relaying. IEEE Communications Letters, 22(10), 2084-2087.
16. Nguyen, X. X., & Do, D. T. (2019). System performance of cooperative NOMA with full-duplex relay over nakagami-m fading channels. Mobile Information Systems, https://doi.org/10.1155/2019/7547431.
17. Tregancini, A., Olivo, E. E. B., Osorio, D. P. M., de Lima, C. H., & Alves, H. (2019). Performance Analysis of Full-Duplex Relay-Aided NOMA Systems Using Partial Relay Selection. IEEE Transactions on Vehicular Technology, 69(1), 622-635.
18. Shen, Z., Liu, G., Ding, Z., Xiao, M., Ma, Z., & Yu, F. R. (2019). Optimal Power Allocations for 5G Non-Orthogonal Multiple Access with Half/Full Duplex Relaying. IEEE International Conference on Communications (ICC). https://doi.org/10.1109/ICC.2019.8761923.
19. Mavoungou, S., Kaddoum, G., Taha, M., & Matar, G. (2016). Survey on threats and attacks on mobile networks. IEEE Access, 4, 4543-4572.
20. Zou, Y., Zhu, J., Wang, X., & Hanzo, L. (2016). A survey on wireless security: Technical challenges, recent advances, and future trends. Proceedings of the IEEE, 104(9), 1727-1765.
21. Pierrot, A. J., Chou, R. A., & Bloch, M. R. (2013). The Effect of Eavesdropper's Statistics in Experimental Wireless Secret-Key Generation. arXiv, https://arxiv.org/abs/1312.3304.
22. Trappe, W., Howard, R., & Moore, R. S. (2015). Low-energy security: Limits and opportunities in the internet of things. IEEE Security & Privacy, 13(1), 14-21.
23. Shannon, C. E. (1949). Communication theory of secrecy systems. The Bell system technical journal, 28(4), 656-715.

24. Wyner, A. D. (1975). The wiretap channel. Bell system technical journal, 54(8), 1355-1387.
25. Fang, D., Qian, Y., & Hu, R. Q. (2017). Security for 5G mobile wireless networks. IEEE Access, 6, 4850-4874.
26. Ahmad, I., Kumar, T., Liyanage, M., Okwuibe, J., Ylianttila, M., & Gurtov, A. (2018). Overview of 5G security challenges and solutions. IEEE Communications Standards Magazine, 2(1), 36-43.
27. Khan, R., Kumar, P., Jayakody, D. N. K., & Liyanage, M. (2019). A Survey on Security and Privacy of 5G Technologies: Potential Solutions, Recent Advancements, and Future Directions. IEEE Communications Surveys & Tutorials, 22(1), 196-248.
28. Chen, J., Yang, L., & Alouini, M. S. (2018). Physical layer security for cooperative NOMA systems. IEEE Transactions on Vehicular Technology, 67(5), 4645-4649.
29. ELHALAWANY, Basem M., RUBY, Rukhsana, RIIHONEN, Taneli, et al. Performance of cooperative NOMA systems under passive eavesdropping. In : 2018 IEEE Global Communications Conference (GLOBECOM). https://doi.org/10.1109/GLOCOM.2018.8647883.
30. Yu, C., Ko, H. L., Peng, X., & Xie, W. (2019). Secrecy Outage Performance Analysis for Cooperative NOMA Over Nakagami-*m* Channel. IEEE Access, 7, 79866-79876.
31. Abbasi, O., & Ebrahimi, A. (2017). Secrecy analysis of a NOMA system with full duplex and half duplex relay. In 2017 Iran Workshop on Communication and Information Theory (IWCIT), https://doi.org/10.1109/IWCIT.2017.7947676.
32. Feng, Y., Yang, Z., & Yan, S. (2017). Non-orthogonal multiple access and artificial-noise aided secure transmission in FD relay networks. In 2017 IEEE Globecom Workshops (GC Wkshps), https://doi.org/10.1109/GLOCOMW.2017.8269229.
33. Cao, Y., Tang, J., Zhao, N., Chen, Y., Zhang, X. Y., Jin, M., & Alouini, M. S. (2019). Full-Duplex Relay Assisted Secure Transmission for NOMA Networks. In IEEE/CIC International Conference on Communications in China (ICCC), https://doi.org/10.1109/ICCChina.2019.8855860.
34. Cao, Y., Zhao, N., Pan, G., Chen, Y., Fan, L., Jin, M., & Alouini, M. S. (2019). Secrecy analysis for cooperative NOMA networks with multi-antenna full-duplex relay. IEEE Transactions on Communications, 67(8), 5574-5587.
35. Bloch, M., Barros, J., Rodrigues, M. R., & McLaughlin, S. W. (2008). Wireless information-theoretic security. IEEE Transactions on Information Theory, 54(6), 2515-2534.
36. Yacoub, M. D. (2001). The $\kappa - \mu$ distribution: a general fading distribution. In IEEE 54th vehicular technology conference-fall 2001. https://doi.org/10.1109/VTC.2001.956432.
37. Yacoub, M. D. (2007). The - distribution and the - distribution. IEEE Antennas and Propagation Magazine, 49(1), 68-81.
38. Fikadu, M. K., Sofotasios, P. C., Valkama, M., Muhaidat, S., Cui, Q., & Karagiannidis, G. K. (2015). Outage probability analysis of dual-hop full-duplex decode-and-forward relaying over generalized multipath fading conditions. In IEEE 11th International Conference on Wireless and Mobile Computing, Networking and Communications (WiMob), https://doi.org/10.1109/WiMOB.2015.7347992.
39. Simon, M. K., & Alouini, M. S. (2005). Digital communication over fading channels (Vol. 95). John Wiley & Sons.
40. Gradshteyn, I. S., & Ryzhik, I. M. (2015). Table of Integrals, Series, and Products, 8th edn., ed. by D. Zwillinger.
41. Khoolenjani, N. B., & Khorshidian, K. (2009). On the ratio of Rice random variables.
42. Prudnikov, A. P., Brychkov, Y. A., & Marichev, O. I. (1986). Integrals and series, Volume 1: Elementary functions. Gordon&Breach Sci. Publ., New York.
43. Prudnikov, A. P., Brychkov, I. A., & Marichev, O. I. (1986). Integrals and series: special functions (Vol. 2). CRC Press.

Figures

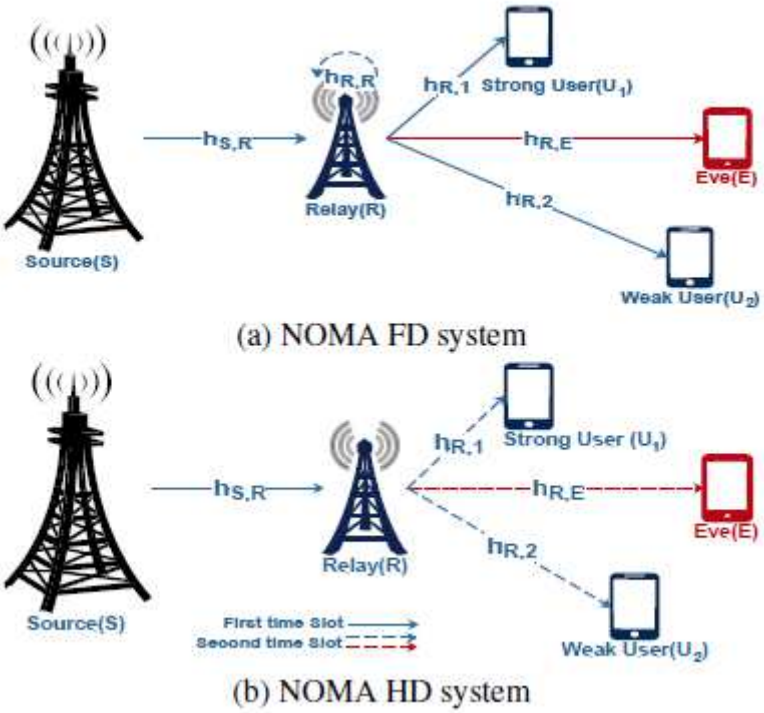

Figure 1

See the Manuscript Files section for the complete figure caption.

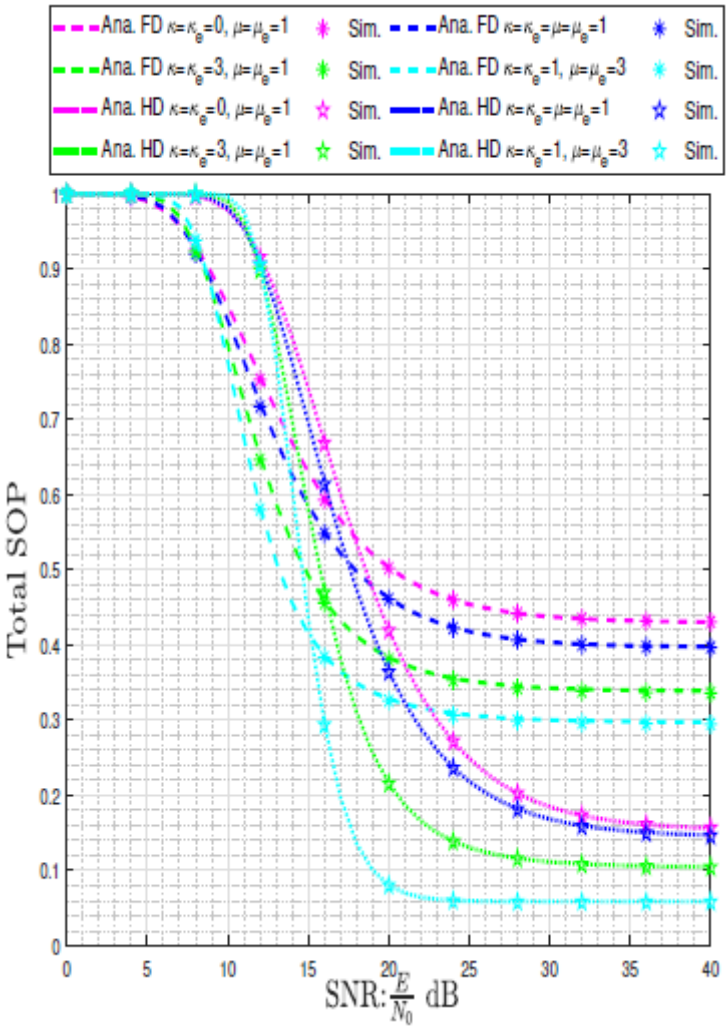

Figure 2

See the Manuscript Files section for the complete figure caption.

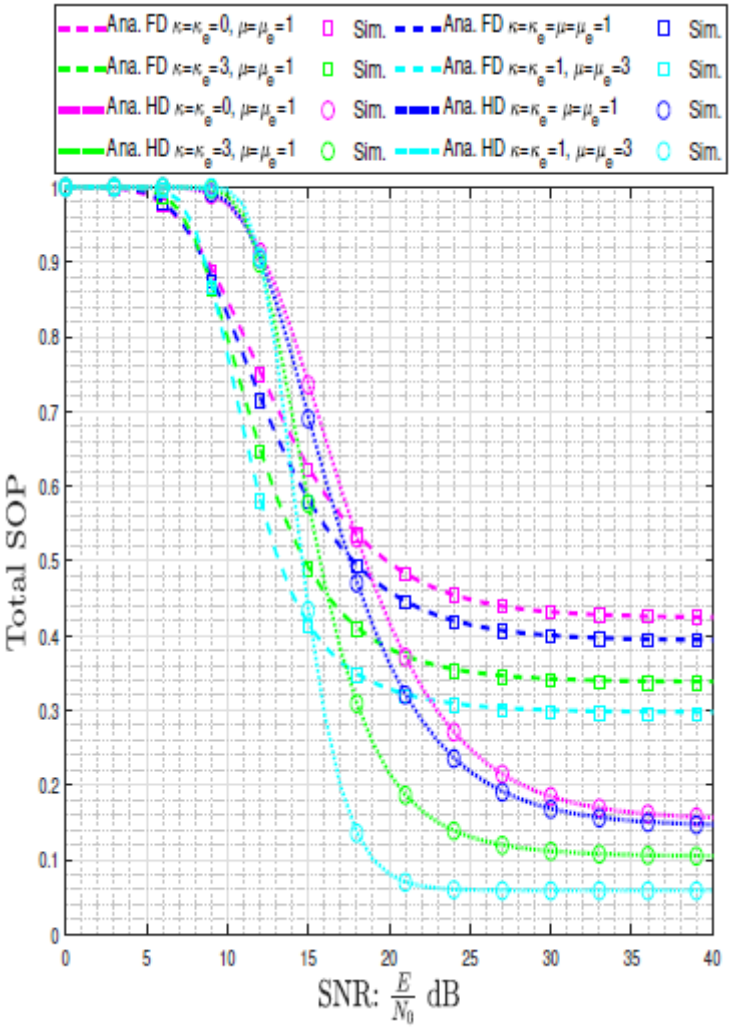

Figure 3

See the Manuscript Files section for the complete figure caption.

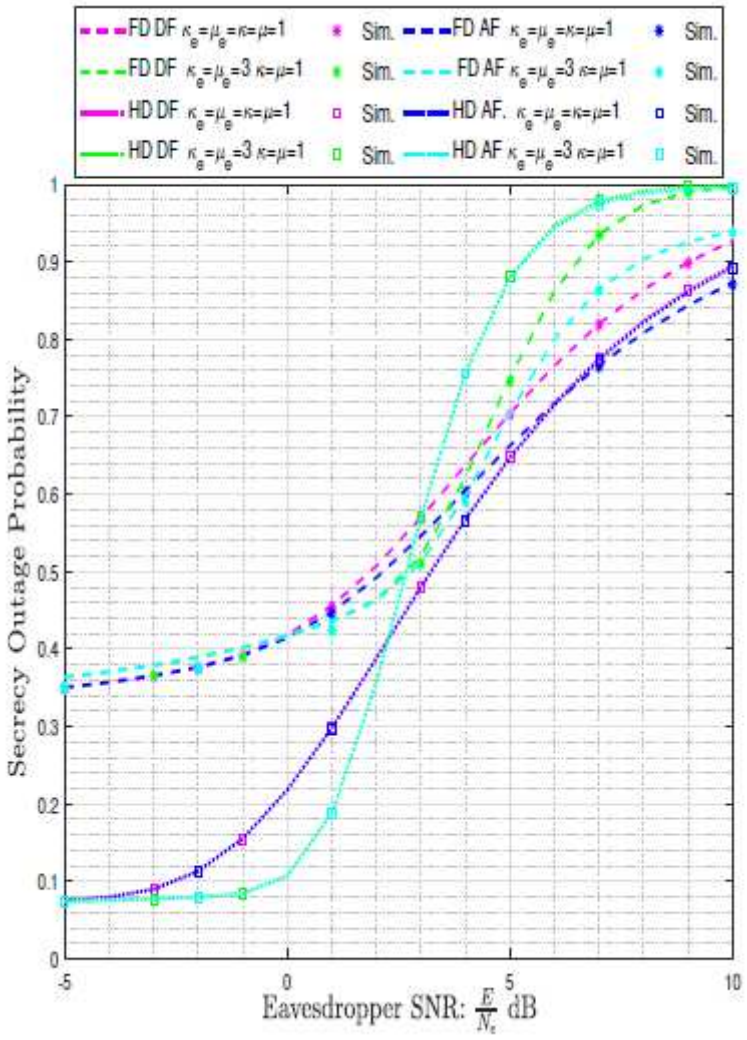

Figure 4

See the Manuscript Files section for the complete figure caption.

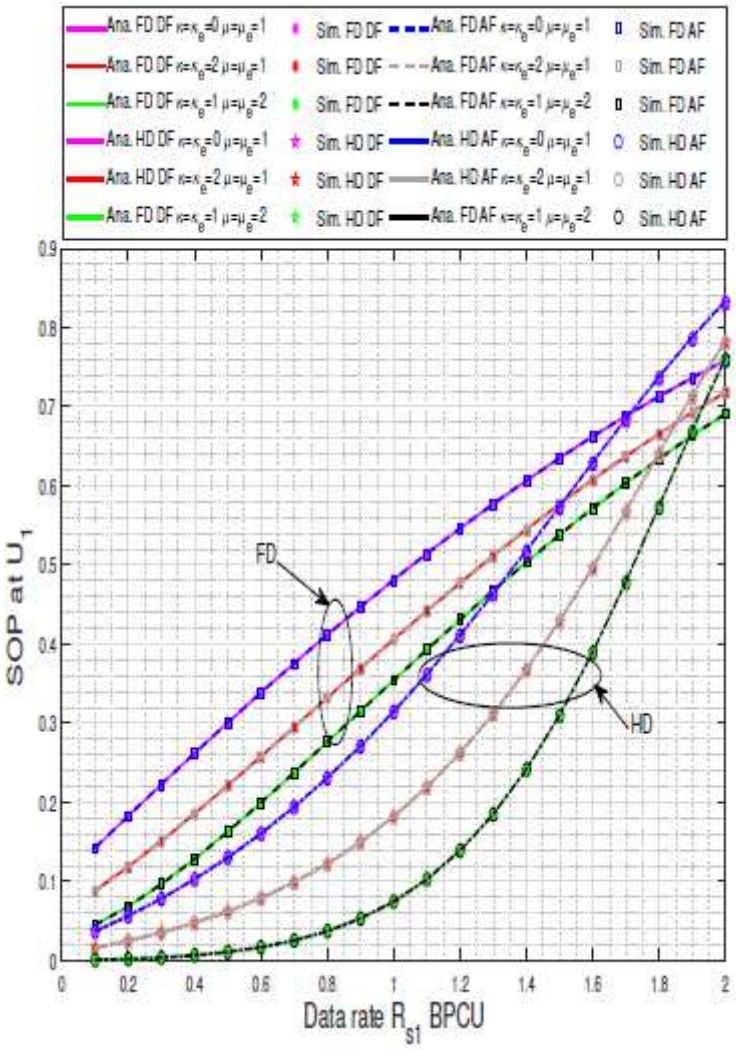

Figure 5

See the Manuscript Files section for the complete figure caption.

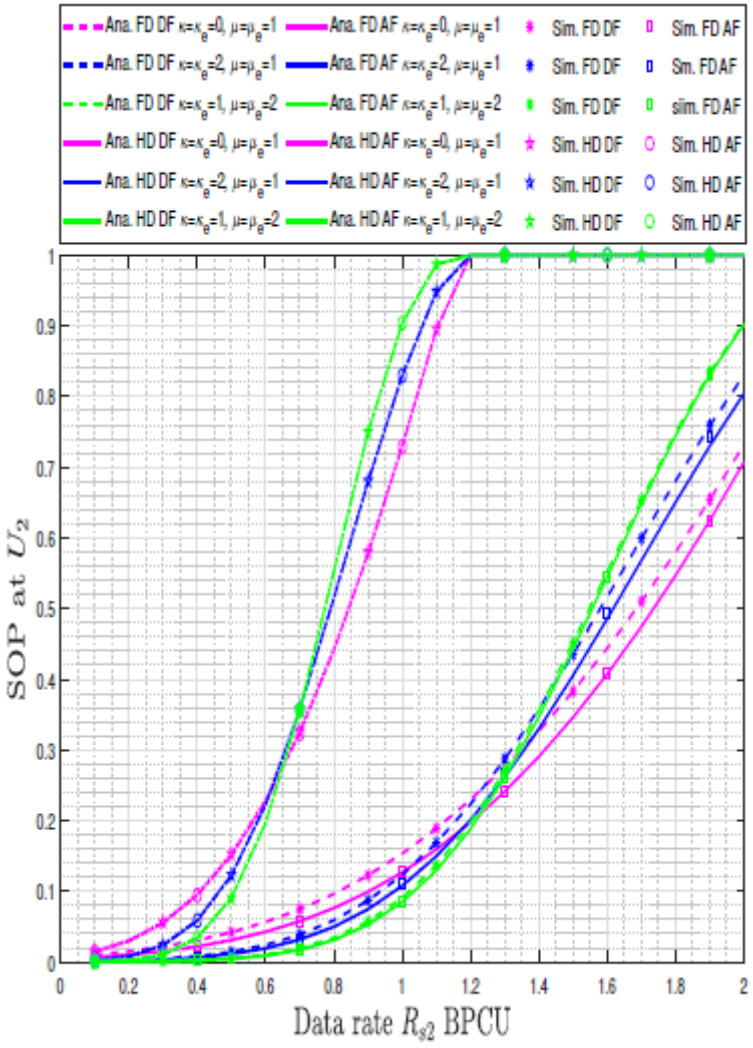

Figure 6

See the Manuscript Files section for the complete figure caption.

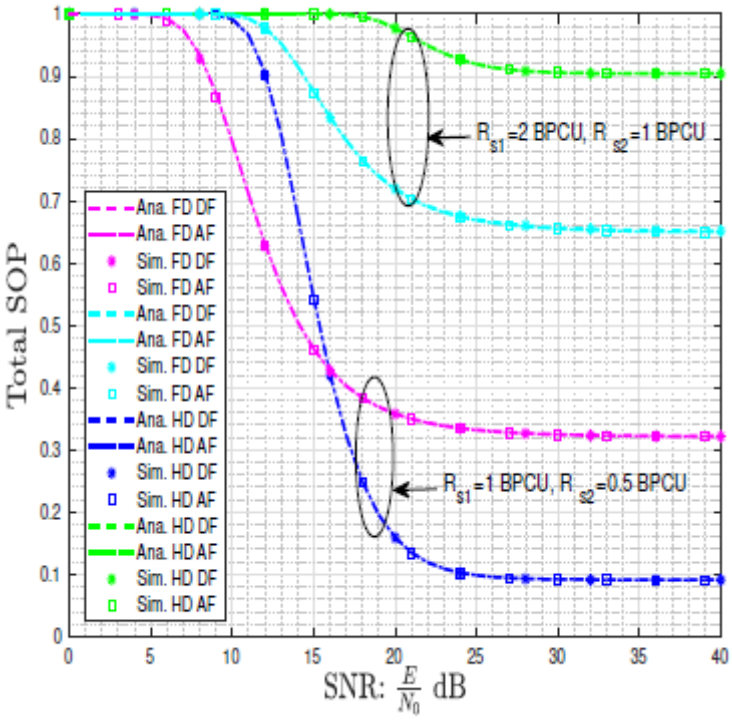

Figure 7

See the Manuscript Files section for the complete figure caption.

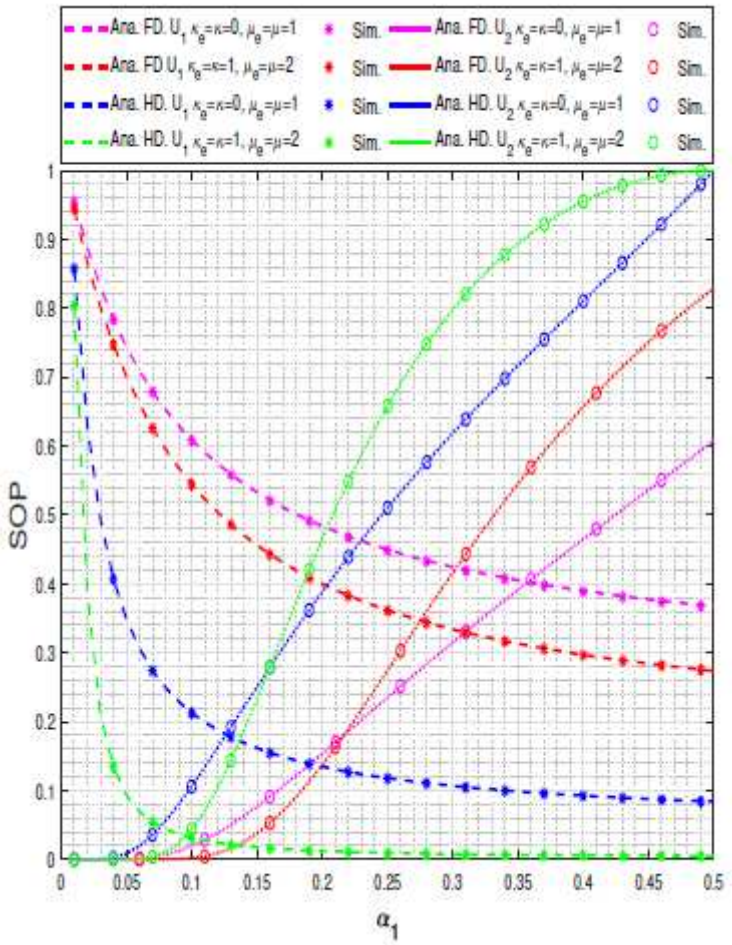

Figure 8

See the Manuscript Files section for the complete figure caption.

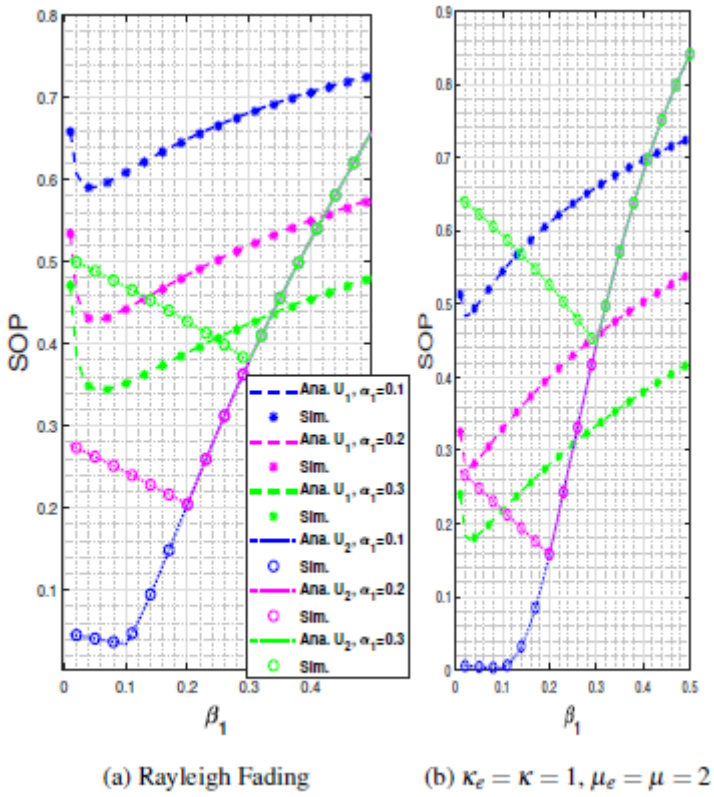

(a) Rayleigh Fading (b) $\kappa_e = \kappa = 1, \mu_e = \mu = 2$

Figure 9

See the Manuscript Files section for the complete figure caption.

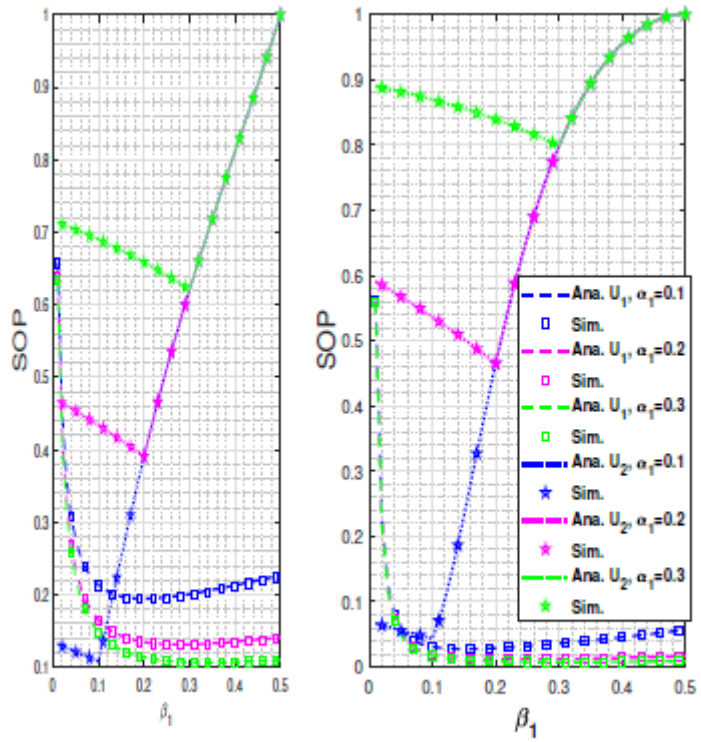

(a) Rayleigh Fading (b) $\kappa_e = \kappa = 1$, $\mu_e = \mu = 2$

Figure 10

See the Manuscript Files section for the complete figure caption.

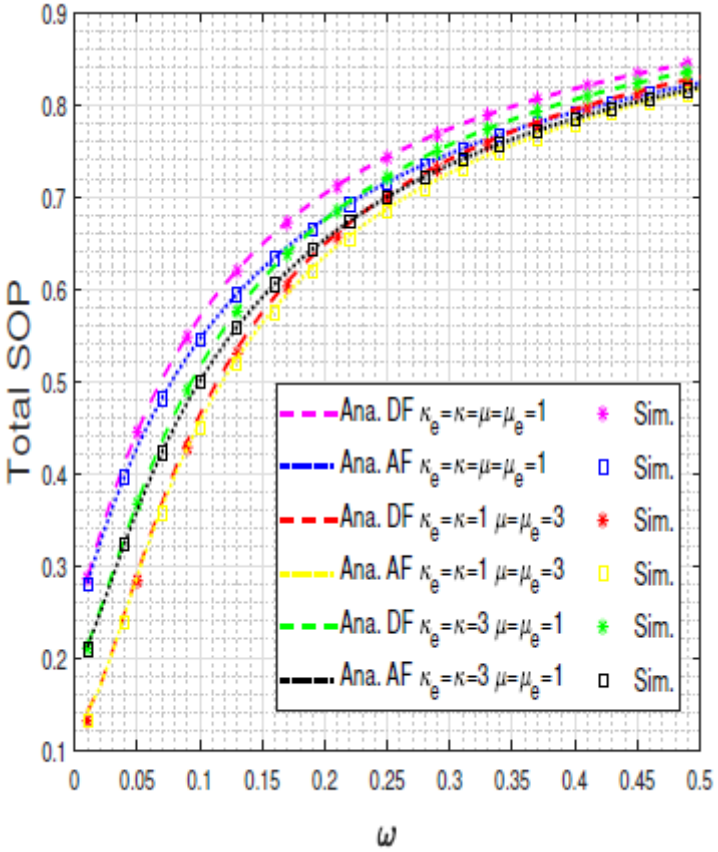

Figure 11

See the Manuscript Files section for the complete figure caption.

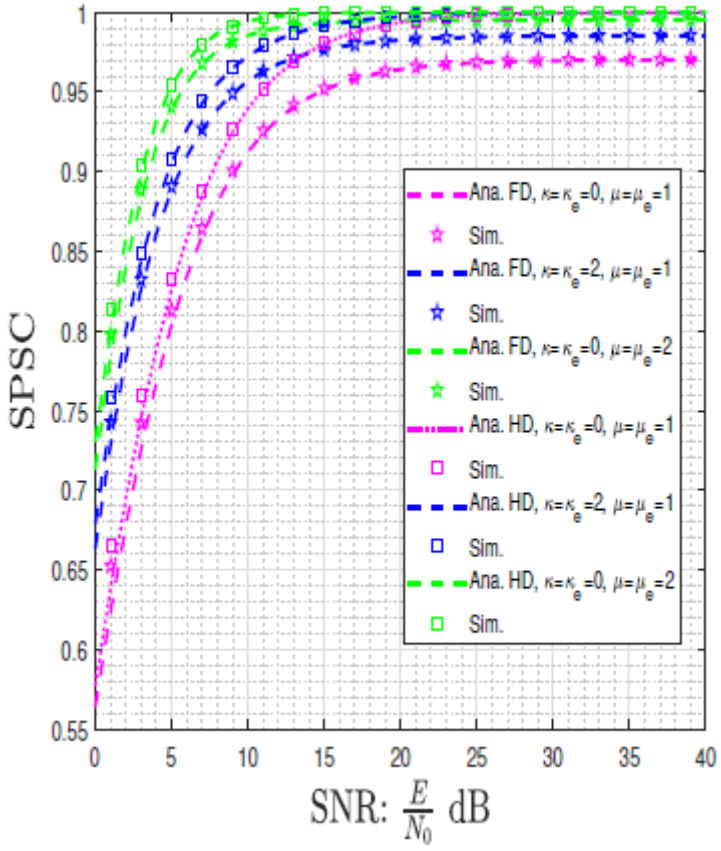

Figure 12

See the Manuscript Files section for the complete figure caption.

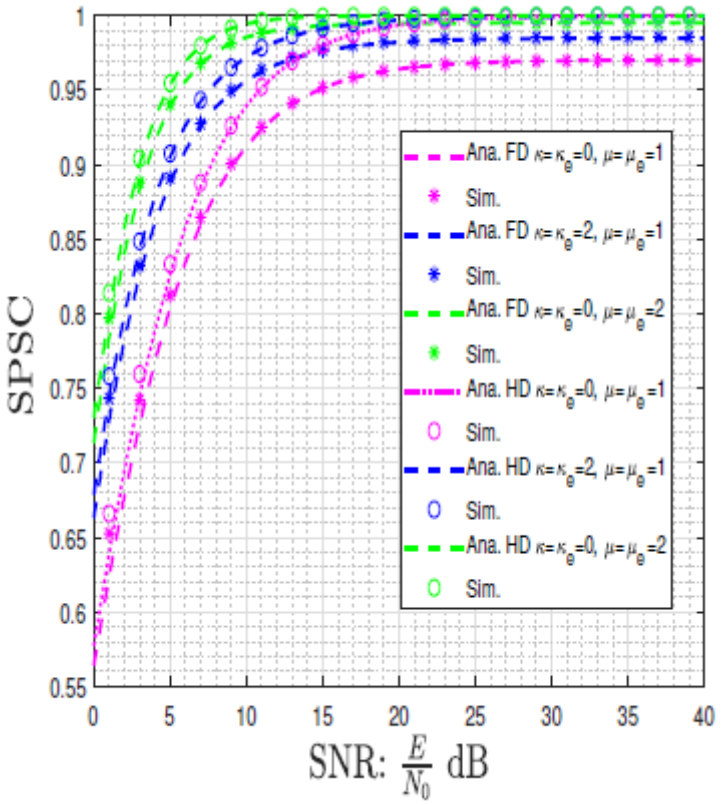

Figure 13

See the Manuscript Files section for the complete figure caption.

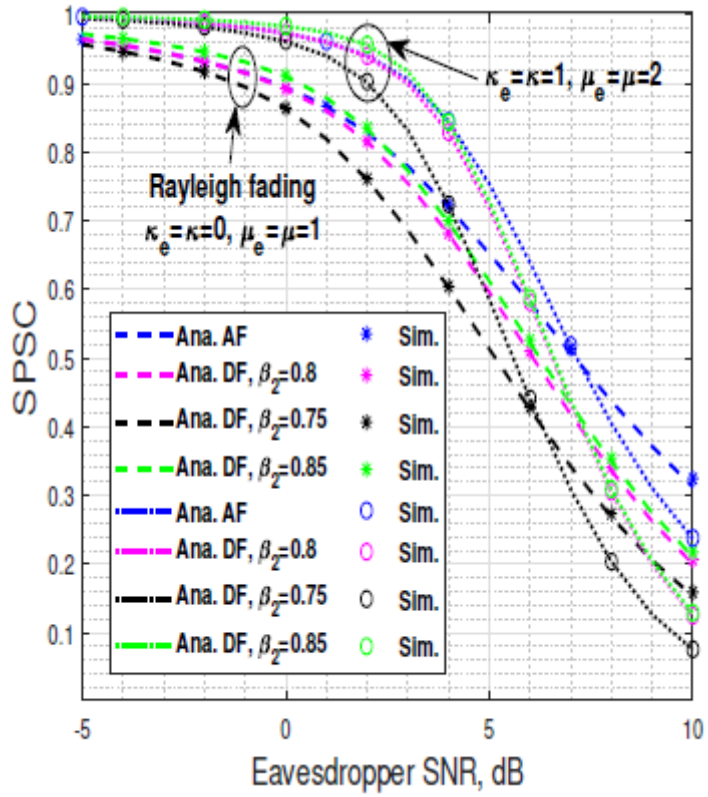

Figure 14

See the Manuscript Files section for the complete figure caption.

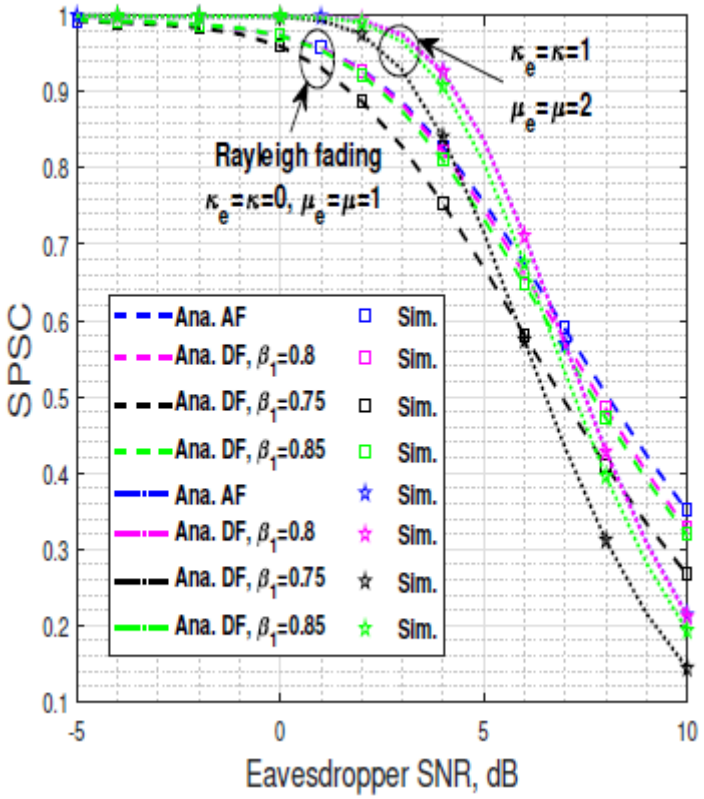

Figure 15

See the Manuscript Files section for the complete figure caption.